Earth and Environmental Science Transactions of the Royal Society of Edinburgh, **111**, 209–233, 2021 (for 2020)

Article

Revision of *Erpetosuchus* (Archosauria: Pseudosuchia) and new erpetosuchid material from the Late Triassic 'Elgin Reptile' fauna based on µCT scanning techniques

Davide FOFFA[1]*, Richard J. BUTLER[2], Sterling J. NESBITT[3], Stig WALSH[1,4], Paul M. BARRETT[5], Stephen L. BRUSATTE[1,4] and Nicholas C. FRASER[1,4]

[1] Department of Natural Sciences, National Museums Scotland, Chambers Street, Edinburgh EH1 1JF, UK
[2] School of Geography, Earth and Environmental Sciences, University of Birmingham, Edgbaston, Birmingham B15 2TT, UK
[3] Department of Geosciences, Virginia Tech, 4044 Derring Hall (MC0420) 926 West Campus Drive, Blacksburg 24061, Virginia, USA
[4] School of GeoSciences, University of Edinburgh, Grant Institute, Hutton Road, Edinburgh EH9 3FE, UK
[5] Department of Earth Sciences, Natural History Museum, Cromwell Road, London SW7 5BD, UK
*Corresponding author. Email: D.Foffa@nms.ac.uk

ABSTRACT: The Late Triassic fauna of the Lossiemouth Sandstone Formation (LSF) from the Elgin area, Scotland, has been pivotal in expanding our understanding of Triassic terrestrial tetrapods. Frustratingly, due to their odd preservation, interpretations of the Elgin Triassic specimens have relied on destructive moulding techniques, which only provide incomplete, and potentially distorted, information. Here, we show that micro-computed tomography (µCT) could revitalise the study of this important assemblage. We describe a long-neglected specimen that was originally identified as a pseudosuchian archosaur, *Ornithosuchus woodwardi*. µCT scans revealed dozens of bones belonging to at least two taxa: a small-bodied pseudosuchian and a specimen of the procolophonid *Leptopleuron lacertinum*. The pseudosuchian skeleton possesses a combination of characters that are unique to the clade Erpetosuchidae. As a basis for investigating the phylogenetic relationships of this new specimen, we reviewed the anatomy, taxonomy and systematics of other erpetosuchid specimens from the LSF (all previously referred to *Erpetosuchus*). Unfortunately, due to the differing representation of the skeleton in the available *Erpetosuchus* specimens, we cannot determine whether the erpetosuchid specimen we describe here belongs to *Erpetosuchus granti* (to which we show it is closely related) or if it represents a distinct new taxon. Nevertheless, our results shed light on rarely preserved details of erpetosuchid anatomy. Finally, the unanticipated new information extracted from both previously studied and neglected specimens suggests that fossil remains may be much more widely distributed in the Elgin quarries than previously recognised, and that the richness of the LSF might have been underestimated.

KEY WORDS: anatomy, Erpetosuchidae, *Erpetosuchus granti*, *Leptopleuron*, systematics.

The fossil reptiles of the Upper Triassic Lossiemouth Sandstone Formation (LSF), from Elgin, Scotland, have been central in revealing the early evolution of modern groups of terrestrial vertebrates (Benton & Walker 1985, 2002, 2011). Unfortunately, studying these specimens, most of which were collected in the 19th Century, is exceedingly difficult because of their preservation as voids (or crumbled bones) in hard sandstone matrix (Benton & Walker 1985). Historically, the 'Elgin reptiles' have been studied using plaster or latex (Walker 1964; Benton & Walker 1985, 2002; Bennett 2020). These traditional techniques often permanently damaged the sandstone blocks containing the fossil and involved deliberate removal of the fragmentary bones to obtain better casts. Furthermore, each new cast changed the morphology of delicate features and has led to ongoing debates about morphology and relationships (Bennett 2020). However, a small number of specimens collected decades ago were left unprepared and their capacity for revealing new information has never been assessed. This unstudied material has the potential to reveal important new information on the anatomy, ecology, relationships and composition of the LSF reptile fauna.

One of these specimens is British Geological Survey (BGS), Geological Survey Museum (GSM) 91072–81, 91085–6. Walker (1964) referred to a partial skeleton visible on the surface of this specimen as a small/juvenile *Ornithosuchus* based on 'the presence of paired dorsal scutes associated with hollow femora' (Walker 1964, p. 55) and the paired row of osteoderms emerging from the matrix. BGS GSM 91072–81, 91085–6 did not receive further attention until Von Baczko & Ezcurra (2016) revised the taxonomy of *Ornithosuchus* and mentioned it among the specimens referred to this genus. This referral was presumably done

 doi:10.1017/S1755691020000109
https://doi.org/10.1017/S1755691020000109 Published online by Cambridge University Press

following Walker (1964), because BGS GSM 91072–81, 91085–6 was not amongst the materials that were studied first-hand by the authors (Von Baczko & Ezcurra 2016, p. 200). Walker (1964) and Von Baczko & Ezcurra (2016), however, had access to only the limited portion of the specimen that is exposed on the surfaces of the blocks, and it has never been clear if other bones were preserved inside. Here, we re-study this specimen using micro-computed tomography (μCT) scanning techniques (Cunningham *et al*. 2014), which reveal a wealth of new bones inside the blocks, including at least two skeletons belonging to different reptiles, neither of which is *Ornithosuchus*. One of these is an erpetosuchid, a clade of archosaurs that belongs within the pseudosuchian lineage that also includes extant crocodylians. In addition to providing key new anatomical information on the rare erpetosuchids, our scans demonstrate that μCT can provide an unprecedented level of anatomical information on the hitherto problematic 'Elgin reptiles'. Along with recent successful computed tomography (CT) scans of the Elgin pseudosuchian *Stagonolepis* (Keeble & Benton 2020), this indicates that previously used destructive techniques will no longer be necessary to study these critically important fossils.

To identify the erpetosuchid specimen contained in the BGS GSM 91072–81, 91085–6 blocks, and conduct an appropriate comparative study, we first needed to revise the diagnosis of the co-occurring pseudosuchian archosaur *Erpetosuchus granti*. Until recently, *E. granti* was the only recognised member of the eponymous family Erpetosuchidae (see Watson 1917; Olsen *et al*. 2001; Benton & Walker 2002; Nesbitt & Butler 2013; Lacerda *et al*. 2018). However, in the last decade, re-evaluation of historical specimens as well as new discoveries from the Middle and Late Triassic of South America and Africa have shown that several features once thought to be unique to *Erpetosuchus* are, in fact, diagnostic of a more speciose erpetosuchid clade (Nesbitt & Butler 2013; Ezcurra *et al*. 2017; Lacerda *et al*. 2018; Nesbitt *et al*. 2018). Unfortunately, the diagnosis of *E. granti* has not been reassessed, and it is unclear how this species can be diagnosed. This issue was initially noticed by Nesbitt & Butler (2013), and has become more problematic with the description of new erpetosuchids, and with our increased understanding of pseudosuchian taxonomy and systematics (Maisch *et al*. 2013; Ezcurra *et al*. 2017; Lacerda *et al*. 2018; Nesbitt *et al*. 2018; Müller *et al*. 2020). Here, we address this problem by revising the diagnosis of *E. granti* based on the available literature (see Ezcurra *et al*. 2017; Supplementary material) and newly obtained μCT data from referred specimens.

Institutional abbreviations. AMNH = American Museum of Natural History, New York, USA; BGS GSM = British Geological Survey, Geological Survey Museum, Keyworth, UK; MCZ = The Louis Agassiz Museum of Comparative Zoology, Harvard University, Cambridge, Massachusetts, USA; NHMUK = Natural History Museum, London, UK; NMS = National Museums Scotland, Edinburgh, UK; NMT = National Museum of Tanzania, Dar es Salaam, Tanzania; SMNS = Staatliches Museum für Naturkunde Stuttgart, Stuttgart, Germany.

1. Materials and methods

The LSF sandstones are composed of white, yellow to pink well-rounded, well-sorted (0.2–0.5 mm) grains of quartz and feldspar with rare clasts of chert and quartzite (Peacock *et al*. 1968; Benton & Walker 1985). Frostick *et al*. (1988) described the LSF deposits as an intercalated sequence of large-scale, cross-bedded aeolian dunes and parallel-bedded, bioturbated lake-shore medium to fine sands. Benton & Walker (1985) recorded that, at Spynie Quarry, the reptiles were recovered stratigraphically low in the quarry, from a layer of friable sandstone near the base of the aeolian dunes, just above a water-laid sands and silts layer. This layer is reported to sit near the base of the LSF in all of the quarries in the Elgin area (Gordon 1859; Murchison 1859; Martin 1860; Benton & Walker 1985, fig. 1).

BGS GSM 91072–81, 91085–6 is a collection of 11 small blocks (from ~5–15 cm in maximum length) of yellow-to-mustard-coloured sandstones from Spynie Quarry (Elgin, Moray), one of many sandstone quarries in the Elgin area (Figs 1, 2). They were 'purchased by Mr Howell (of the Geological Survey) on 14 March 1893' (Walker 1964, p. 56). Little information is available on the state of these blocks at the time of purchase, but it is implied that the blocks were already separated when Walker (1964) studied them. Walker (1964) noted that several of these pieces fitted together (Figs 1, 2) and were linked by the 'peculiar preservation of the matrix' (Walker 1964, pp. 55–56) confirming that they belonged together. One of us (DF) verified that the blocks fit together in two groups: BGS GSM 91080–1, 91085–6 and, on the other side, BGS GSM 91072–79, 91086 (Figs 1, 2). The fit between these two groups is less certain; other blocks from this sequence (presumably including blocks with the missing numbers BGS GSM 91083–84) probably linked the two groups originally. Unfortunately, we were unable to locate these additional blocks – it is likely that they went missing before Walker studied these materials as they were not mentioned in his description ('GSM 91072–78, 91081–82, 91085–86': Walker 1964, p. 55). Some blocks have been glued together, so it is possible that BGS GSM 91083–84 are currently stuck to others (DF, pers. obs. 2019). It is also possible that the fit between the two groups of blocks has been rendered imperfect by the mechanical preparation evident from some of the blocks' surfaces. Nevertheless, the internal content of the blocks, as revealed by μCT scanning, corroborates the conclusion that they all belong together. Focusing on the two most complete skeletons preserved within the blocks, we notice that there is no duplication of bone elements (i.e., no element is represented more than once) between the two groups and that comparable elements (e.g., osteoderms) are identical in size and morphology in the separate blocks (Fig. 2). Indeed, the presumed cervical–dorsal vertebrae and distal tail of this individual is in BGS GSM 91072–79, 91086, whereas the posterior dorsal, sacral and anterior–middle caudal vertebrae and hindlimbs are all in BGS GSM 91080–1, 91085. The arch-like orientation of the dorsal to caudal vertebral series hints at the original relationship of the blocks to one another, as depicted in Figures 1 and 2, which matches the tentative arrangement based on the broken sandstone surface.

It is convenient at this point to simplify the nomenclature of BGS GSM 91072–82, 91085–6. BGS assigned an individual register number to each sandstone block, but this nomenclature cannot be used easily herein because the μCT scans show that the skeletons of at least two individuals of distinct species are embedded within them. The first of these belongs to a pseudosuchian archosaur – the specimen that is currently referred to *Ornithosuchus woodwardi* (Walker 1964; Von Baczko & Ezcurra 2016) – and is partially exposed on the surfaces of the blocks; the second is a previously undocumented partial skeleton of the procolophonid *Leptopleuron lacertinum* (also known from the LSF fauna) (Benton & Walker 1985; Säilä 2010). For example, BGS GSM 91075 contains both cranial material of the archosaur and the *L. lacertinum* remains. Thus, for simplicity, we will use 'BGS GSM Elgin A' ('A' standing for 'archosaur') to refer to the archosaur skeleton in BGS GSM 91072–82, 91085–6, which is the focus of this manuscript. The second skeleton in the same blocks will be referred as to 'BGS GSM Elgin P' (for 'procolophonid'), and is separately described along with additional unidentified bones. We use specific BGS register numbers to reference individual sandstone blocks, in order to specify where each bone is preserved.

https://doi.org/10.1017/S1755691020000109 Published online by Cambridge University Press

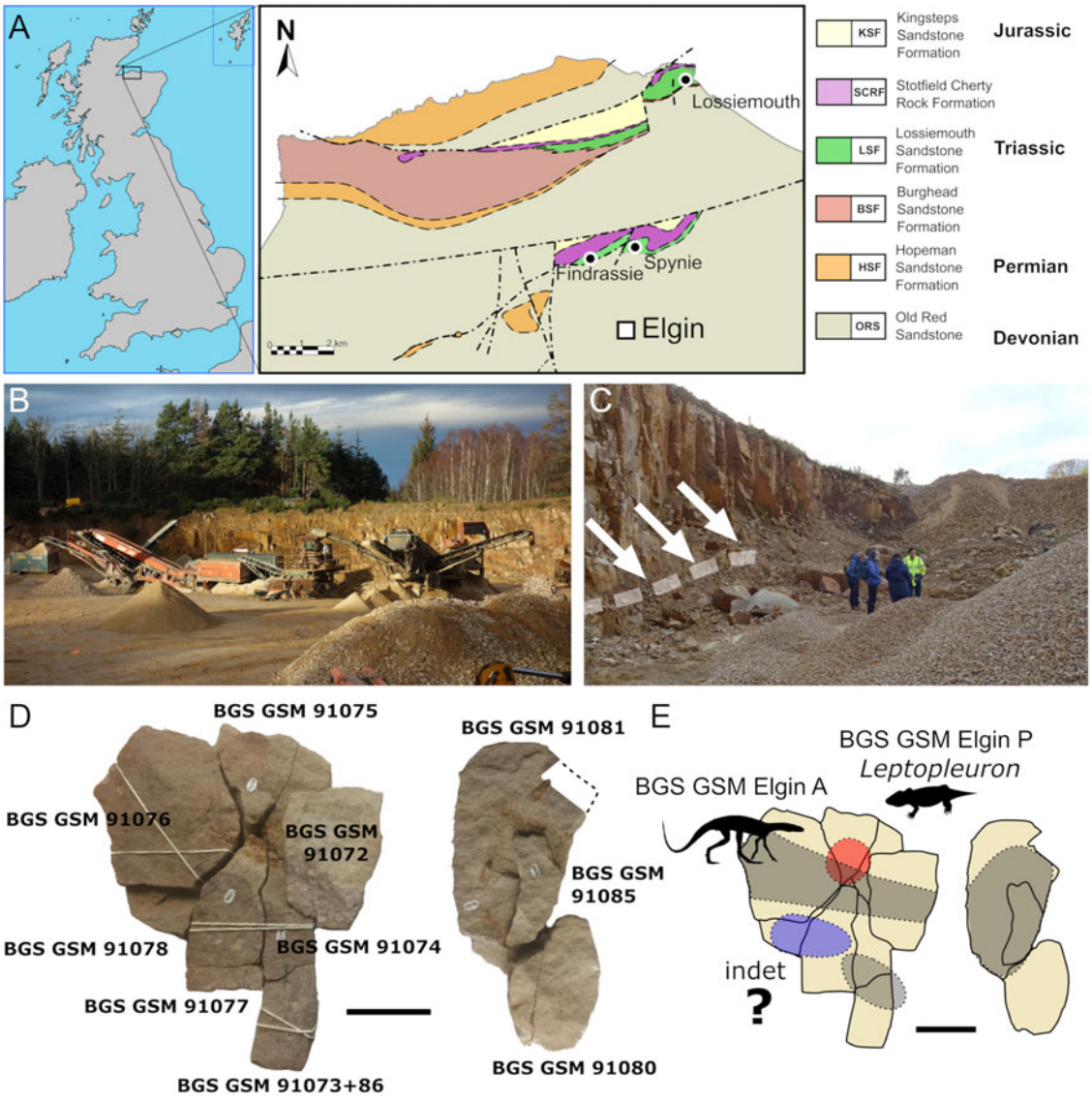

Figure 1 (A) Map of Great Britain showing the position of the 'Elgin' quarries, with a geological map of the Elgin area (Moray, Scotland, UK); (B, C) field photographs of the Spynie quarries, with white arrows and dashed line indicating the fossiliferous layer identified on one of the active faces of the quarry; (D) photographs of the articulated blocks comprising BGS GSM 91072–81, 91085–6; (E) schematic representations of the distribution of the fossil content (each colour corresponds to a different individual) in the sandstone blocks. The geological map was redrawn from Benton & Walker (1985). Silhouettes from www.phylopic.org. Scale bars = 5 cm (D, E).

1.1. µCT scanning methods

BGS GSM 91072–81, 91085–6 (Figs 1, 2) were scanned with the assistance of Dr Tom G. Davis and Dr Elizabeth Martin-Silverstone using a Nikon XT H 225 µCT scanner at the Palaeobiology Lab of the University of Bristol. To increase resolution by reducing the field of view, the ten blocks of BGS GSM 91072–81, 91085–6 were scanned separately in six groups (Figs 1D, E, 2; Table 1) (supplemental Table S1). During the scanning, some of the blocks were held together with rubber bands to maintain their original association (some bones, such as the quadrate, are split between blocks). Given the limited dimensions of the samples, this procedure did not significantly affect the resolution of the scans, which vary from 0.023 to 0.073 mm (isometric voxel size) depending on the size of each block (see supplementary Table S1 for individual scan parameters).

Blocks containing a referred specimen of *Erpetosuchus granti* (NMS G.1992.37.1) (Figs 3, 4) were scanned for comparative purposes with the assistance of Dr Alice Macente and SW. The scanning took place at the µCT facility (Nikon XT H 225 µCT) hosted in the Advanced Materials Research Laboratory of the Civil and Environmental Engineering Department at the University of Strathclyde, and shared with the School of Earth and Geographical Science of the University of Glasgow. The resolution of these datasets varies from 0.0624 to 0.0678 mm (isometric voxel size) (Table 1) (see supplementary Table S1 for individual scan parameters).

The CT dataset of *Erpetosuchus* sp. (AMNH 29300) (Fig. 5) was acquired by one of the authors (SLB) in Autumn 2012 at the Microscopy and Imaging Facility at AMNH with the assistance of Morgan Hill (Table 1) (see supplementary Table S1 for individual scan parameters).

All the µCT datasets were segmented using Mimics 21.0 (https://www.materialise.com/mimics). The three-dimensional (3D) models and µCT datasets were uploaded to Morphosource (https://www.morphosource.org/) and can be accessed at [https://www.morphosource.org/MyProjects/Dashboard/dashboard/select_project_id/1115], following the recommendations on sharing digital data proposed by Davies *et al.* (2017). The small size of the bones in the BGS specimens may raise questions about the confidence with which we are presenting interpretations of our data. We were able to segment extremely small structures thanks to the reduced physical size of the samples (approximately

https://doi.org/10.1017/S1755691020000109 Published online by Cambridge University Press

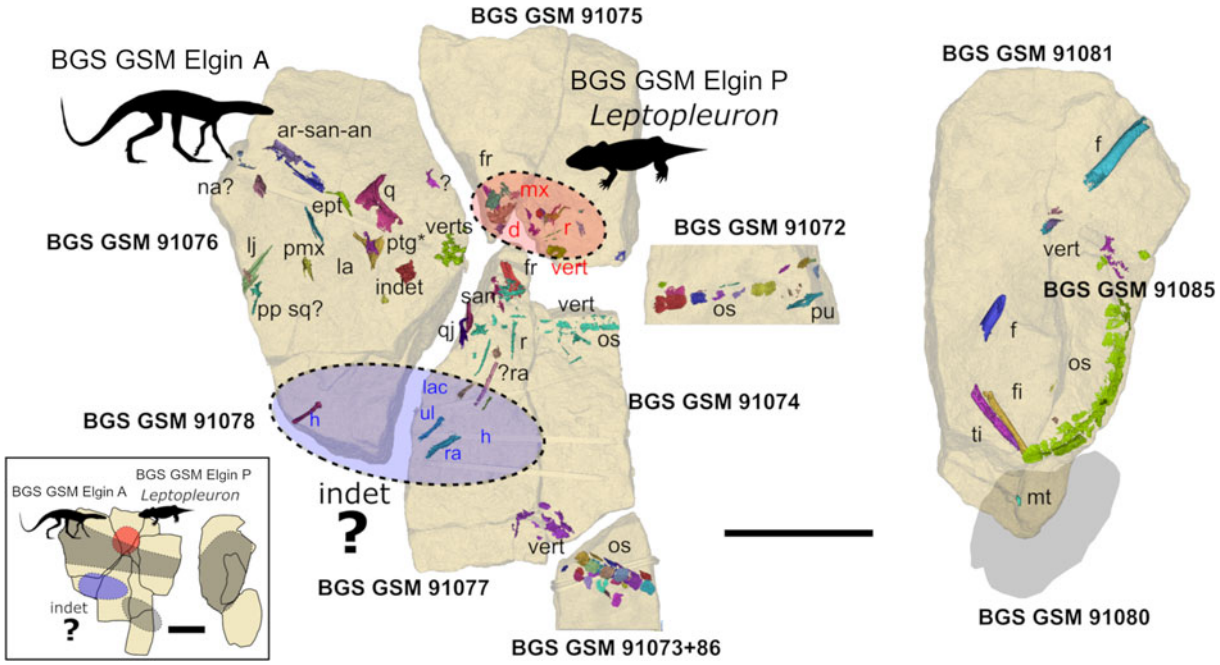

Figure 2 Detailed fossil content of BGS GSM 91072–81, 91085–6 based on the digital reconstruction following the μCT scanning and segmentation. Abbreviations: an = angular; ar = articular; d = dentary; ept = ectopterygoid; f = femur; fi = fibula; fr = frontal; h = humerus; la = lacrimal; lj = lower jaw; mt = metatarsal; mx = maxilla; na = nasal; os = osteoderm; pmx = premaxilla; pp sq = paroccipital process of the squamosal; pt = pterygoid; pu = pubis; q = quadrate; r = rib; ra = radius; san = surangular; ti = tibia; ul = ulna; vert = vertebra. In the inset figure, bones are colour-coded to show their distributions within the original composite block: black for BGS GSM Elgin A; red for BGS GSM Elgin P; blue for indeterminate. Scale bars = 5 cm.

$10 \times 10 \times 4$ cm for the largest block), small voxel size and the strong contrast between the bones/cavities and the sandstone in the Elgin (BGS and NMS) specimens (supplementary Fig. S1). This combination made it possible to segment the specimens with great accuracy and allowed interpretation of details, in some cases, even without post-processing (e.g., smoothing) the segmented models. This is important because we were able to avoid possible post-processing artefacts that could affect our interpretation of the anatomy and, consequently, the information coded in the phylogenetic analyses.

1.2. Phylogenetic analysis

To test the phylogenetic relationships of BGS GSM Elgin A, we updated the dataset of Müller *et al.* (2020), which incorporates the most recent iterations made to the original dataset of Ezcurra (2016), including modifications implemented in Ezcurra *et al.* (2017). This dataset was selected because it contains the most complete sampling of erpetosuchid species. Before conducting our analysis, we modified the taxon/character matrix by adding four terminal taxa and updated the scores of two others (see Supplementary material). Specifically, in addition to BGS GSM

Table 1 μCT specifications and fossil content of BGS GSM 91072–82, 91085–6 blocks, *Erpetosuchus granti* (NMS G.1992.37.1A-B) and *Erpetosuchus* sp. (AMNH 29300). For further μCT details, see supplementary Table S1 and [https://www.morphosource.org/MyProjects/Dashboard/dashboard/select_project_id/1115].

Specimen number	Voxel size [mm]	Fossil content
BGS GSM 91081, 91085	0.0836	BGS GSM Elgin A: femora, tibia, fibula, metatarsals, sacral and caudal vertebrae and associated series of osteoderms
BGS GSM 91086, 91073	0.0234	BGS GSM Elgin A: middle-posterior caudal series and associated rows of osteoderms
BGS GSM 91072	0.0390	BGS GSM Elgin A: posterior dorsal osteoderms, ?pubis and associated vertebral fragments
BGS GSM 91075	0.0489 and 0.0248 (close-up)	BGS GSM Elgin A: frontal (l) BGS GSM Elgin P: anterior snout (dentary, maxilla, premaxilla, teeth), associated skull and vertebral fragments, ribs
BGS GSM 91077, 91074	0.0618	BGS GSM Elgin A: frontal (r), quadratojugal, surangular, ribs, dorsal vertebral fragments and associated osteoderms, ?radius INDET: humerus, radius, ulna, ?lacrimal
BGS GSM 91076, 91078	0.0733 and 0.0369 (close-up)	BGS GSM Elgin A: ?nasal/maxilla, lower jaw fragments, quadrate, ?squamosal, lacrimal, pterygoid, ectopterygoid BGS GSM Elgin P: skull roof INDET: humerus
BGS GSM 91080–2, 91085	N/A	N/A
NMS G.1992.37.1A-B	0.0624 (A) and 0.0678 (B)	*Erpetosuchus granti*: (A) right side of cervical–(anterior) dorsal vertebrae with associated ribs and series of paramedian and lateral osteoderms, pectoral girdle, complete right forelimb (missing phalanges); (B) left side of and the same, but with only a partial left humerus
AMNH 29300	0.0678	*Erpetosuchus* sp.: right articulated side of a partial skull, and posterior right ramus of lower jaw (see Olsen *et al.* 2001)

https://doi.org/10.1017/S1755691020000109 Published online by Cambridge University Press

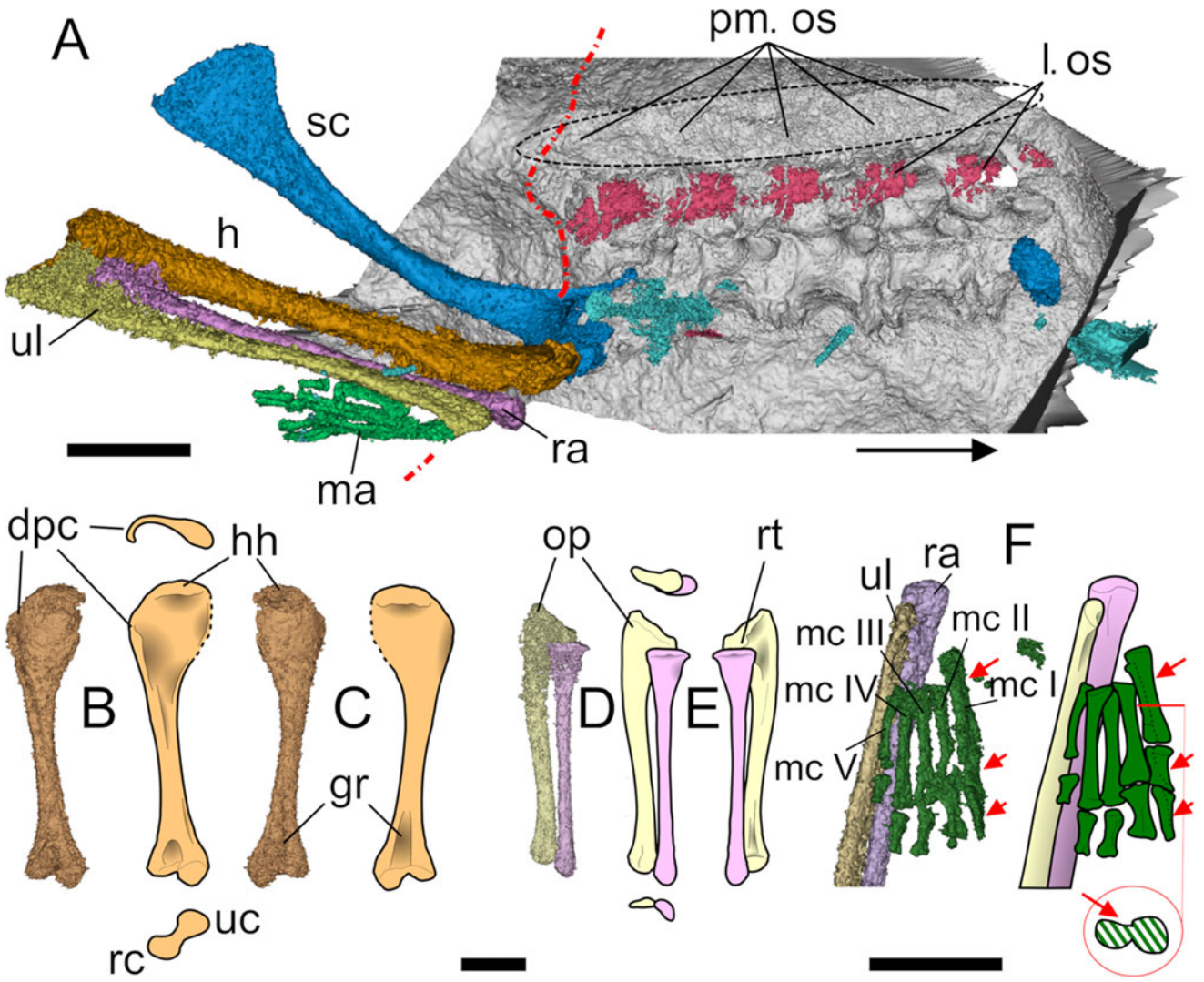

Figure 3 *Erpetosuchus granti*, NMS G.1992.37.1 (referred specimen). (A) Cervical vertebrae, right pectoral girdle and articulated forearm in right lateral view. (B–F) Details of humerus, radius, ulna and manus: (B, C) humerus digital model and line drawing in anterior (middle row), proximal (top), distal (bottom) and posterior views; (D, E) radius and ulna digital model and line drawings; (D) anterior (middle row); (E) proximal (top); and distal (bottom) views; (F) forearm digital model, line drawing and detail showing the cross-section of pathologic metacarpal I. The red arrows indicate the pathology on metacarpal I. Abbreviations: dpc = deltopectoral crest; g = groove; h = humerus; hh = humeral head; l. os = lateral osteoderms; ma = manus; mc I-V = metacarpal I to V; oc = olecranon process; pm. os = paramedian osteoderm; ra = radius; rc = radial condyle; rt = radial tuberosity; sc = scapula; uc = ulnar condyle; ul = ulna; vert = vertebra. Scale bars = 10 mm.

Elgin A, we scored the two most complete specimens of *Parringtonia gracilis* (NMT RB426, NMT RB460: Nesbitt *et al*. 2018) (see supplementary Fig. S2). We also updated the scores of *Erpetosuchus granti* based on direct examination of multiple generations of casts of the holotype specimen (NHMUK PV R3139), and newly acquired µCT scans of a referred specimen (NMS G.1992.37.1). This resulted in the rescoring of 52 character states, including new information on the cervical–dorsal vertebral series, osteoderms, pectoral girdle and forelimbs for *E. granti* (see Supplementary material). Finally, we updated the scores for *Erpetosuchus* sp. (AMNH 393000), also based on CT scans (see Supplementary material). The inclusion of new information from *E. granti* and the addition of better preserved *P. gracilis* specimens increases knowledge of the osteology (particularly postcranial) of the group, which is still poorly understood due to the scarcity of complete specimens (Nesbitt & Butler 2013; Lacerda *et al*. 2018).

The final version of the matrix includes 676 characters and 113 terminal taxa. Ten taxa – *Eorasaurus olsoni*, *Archosaurus rossicus*, *Vonhuenia fredericki*, *Chasmatosuchus rossicus*, *Chasmatosuchus magnus*, '*Chasmatosuchus*' *vjushkovi*, *Kalisuchus rewanensis*, *Shansisuchus kuyeheensis*, *Uralosaurus magnus* and *Koilamasuchus gonzalezdiazi* – were excluded *a priori* (see Ezcurra 2016 for justifications for the exclusions of these taxa). The following characters were treated as additive: 1, 2, 7, 10, 17, 19, 20, 21, 28, 29, 36, 40, 42, 50, 54, 66, 71, 75, 76, 122, 127, 146, 153, 156, 157, 71, 176, 177, 187, 202, 221, 227, 263, 266, 279, 283, 324, 327, 331, 337, 345, 351, 352, 354, 361, 365, 370, 377, 379, 398, 410, 424, 430, 435, 446, 448, 454, 458, 460, 463, 472, 478, 482, 483, 489, 490, 504, 510, 516, 529, 537, 546, 552, 556, 557, 567, 569, 571, 574, 581, 582, 588, 648, 652 and 662. The analysis was performed in TNT v. 1.5 (Goloboff *et al*. 2008) using equally weighted parsimony. The tree space was generated and searches for the most parsimonious trees (MPTs) were conducted using the following protocol: 'New Technology search' (Sectorial Search, Ratchet, Drift and Tree fusing) with 1000 random-addition replicates (RAS). Each method was run for 100 replicates/cycles/iterations. A final round of tree bisection reconnection (TBR) branch swapping was performed after the New Technology search, with a 50% collapsing rule. This procedure retrieved the same results as the protocol followed by Müller *et al*. (2020) that relies instead on 'Traditional search' (RAS +

https://doi.org/10.1017/S1755691020000109 Published online by Cambridge University Press

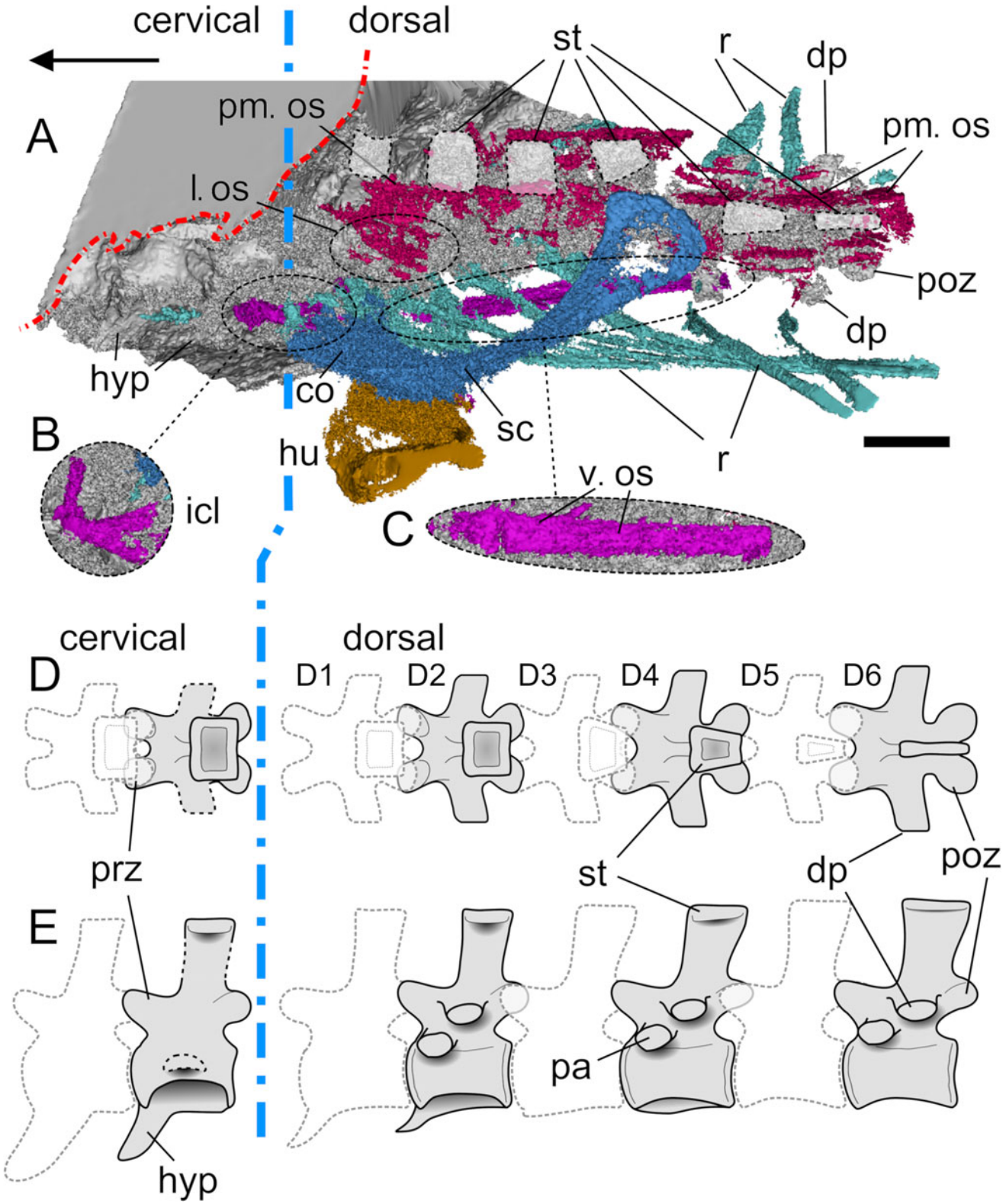

Figure 4 *Erpetosuchus granti*, NMS G.1992.37.1 (referred specimen). (A) Cervical–dorsal vertebrae, left pectoral girdle and articulated forearm in oblique dorsolateral view; (B) close-up of the interclavicle; (C) close-up of the ventral osteoderm row; (D, E) schematic reconstruction of the posterior cervical and anterior dorsal vertebral series in dorsal (top) and lateral (bottom) views. Abbreviations: co = coracoid; D1–6 = first to sixth dorsal vertebra; dp = diapophysis; hu = humerus; hyp = hypapophysis; icl = interclavicle; l. os = lateral osteoderm; pa = parapophysis; pm. os = paramedian osteoderm; poz = postzygapophysis; prz = prezygapophysis; r = rib; sc = scapula; st = spine table; v. os = ventral osteoderm. Scale bar = 10 mm.

TBR) with 1000 replicates of Wagner trees (random seed = 0), and TBR and branch swapping (with ten trees saved per replicate). As in previous analyses, *Petrolacosaurus kansensis* was used to root the MPTs.

2. Systematic palaeontology

Archosauria Cope, 1869, *sensu* Gauthier & Padian 1985
Pseudosuchia Zittel, 1887–1890, *sensu* Sereno *et al.* 2005

https://doi.org/10.1017/S1755691020000109 Published online by Cambridge University Press

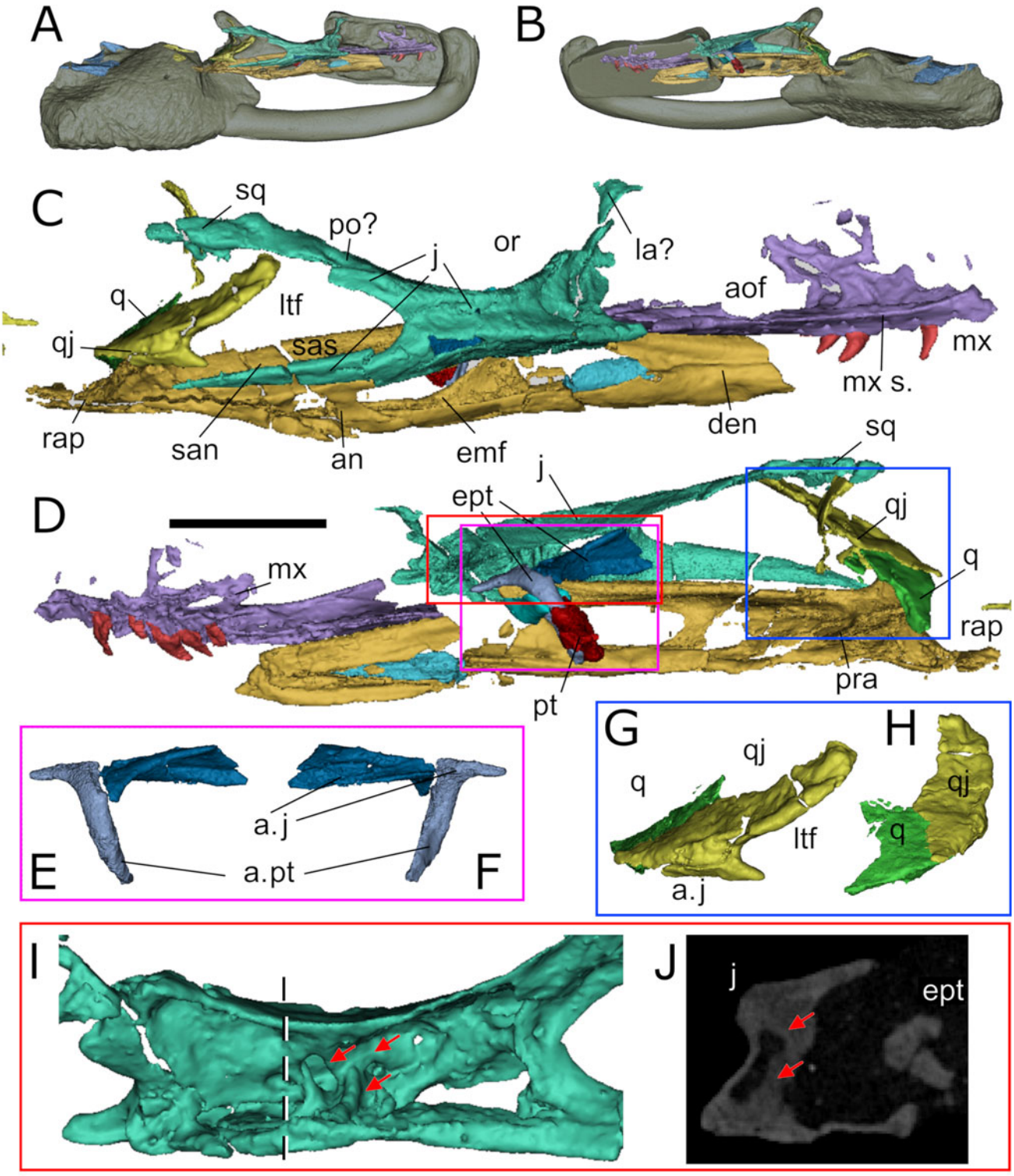

Figure 5 *Erpetosuchus* sp. AMNH 29300. (A) lateral; (B) medial views; (C, D) close-up of the skull in lateral and medial views; (E, F) ectopterygoid in medial and lateral views; (G, H) quadrate and quadratojugal in lateral and posterior views; (I, J) jugal in medial view and coronal section as seen in the μCT scans. The red arrows indicate pneumatic structures (cavities and trabeculae) of the jugal. Abbreviations: a.j = articulation for the jugal; an = angular; aof = antorbital fenestra; a.pt = articulation for the pterygoid; den = dentary; emf = external mandibular fenestra; ept = ectopterygoid; la = lacrimal; ltf = lower temporal fenestra; mx = maxilla; mx s. = maxillary shelf; or = orbit; po = postorbital; pra = prearticular; pt = pterygoid; q = quadrate; qj = quadratojugal; rap = retroarticular process; san = surangular; sas = surangular shelf; sq = squamosal. Scale bar = 10 mm (C, D).

Suchia Krebs, 1974, *sensu* Nesbitt 2011
Erpetosuchidae Watson, 1917, *sensu* Nesbitt & Butler 2013
Erpetosuchus granti Newton, 1894.

Type specimen. NHMUK PV R3139, consisting of the natural mould of a complete skull and mandible, articulated series of cervical and anterior dorsal vertebrae, and the shoulder girdle and forelimbs. Associated with this specimen are different generations of casts: Newton's original gutta percha casts are BGS GSM 91029–91051; the PVC and Vinagel casts made by Walker are located with NHMUK PV R3139 (see Benton & Walker 2002).

Referred material. NMS G.1992.37.1 articulated series of cervical and anterior dorsal vertebrae, associated with paramedian and lateral osteoderms, ribs and the shoulder girdle and forelimbs (complete right forelimb, only missing its distal phalanges,

https://doi.org/10.1017/S1755691020000109 Published online by Cambridge University Press

and incomplete left humerus); NMS G.1966.43.4, partial dorsal vertebral region, with associated paramedian and lateral osteoderms and ribs.

Locality and horizon. The type specimen of *E. granti* was collected from the breakwater at Lossiemouth, near Elgin (Moray, Scotland, UK) and it originated from either Spynie or the Lossiemouth quarries. NMS G.1992.37.1 was found in a block on the beach near Lossiemouth old rail station, likely from the material discarded by the Lossiemouth quarries. NMS G.1966.43.4 is part of the Stollery Collection at the NMS, obtained from Mr E. Stollery of Sandend (Cullen); its precise provenance is unknown. All of the specimens come from aeolian sandstones of the LSF (Upper Triassic: ~upper Carnian/lower Norian: but see Benton & Walker 2011).

Other potentially referable material. NHMUK PV R4807 is a series of 16 articulated vertebrae from Lossiemouth, but this specimen cannot be referred to *Erpetosuchus* unambiguously (see Benton & Walker 2002). AMNH 29300 is a partial skull from the New Haven Formation of Connecticut (Hartford Basin, Newark Supergroup) (Upper Triassic: ~upper Carnian/lower Norian; but see Olsen *et al*. 2001). This specimen is referred to *Erpetosuchus* sp. and is redescribed separately (see below).

Emended diagnosis. *Erpetosuchus granti* differs from all other erpetosuchids in (* indicates local autapomorphies): having a snout that tapers anteriorly in lateral view; obtuse angle (~105°) between the alveolar and anterior margins of the premaxilla* (unique within Erpetosuchidae); 4–5 maxillary teeth; teeth without carinae posterior process of the quadratojugal is thin and strongly elongated (anteroposterior length/vertical depth at the base >4; shared with *Erpetosuchus* sp. (AMNH 29300)); strongly elongated scapula (total length/minimum anteroposterior width of the scapular blade >13)* (unique within Pseudosuchia); well-developed trapezoidal hypapophyses on the middle–posterior cervical and anterior dorsal vertebrae (based on NMS G.1992.37.1); spine tables (and pit) present on the dorsal surface of the neural spine on the cervical and anterior dorsal vertebrae and absent from the middle dorsals (based on NMS G.1992.37.1); paramedian and lateral osteoderms longer than wide and with a distinct keel (shared with *Parringtonia gracilis*); paramedian osteoderms with unornamented anterior articular lamina (shared with *Archeopelta arborensis* and *P. gracilis*).

Comments. Six autapomorphies were used by Benton & Walker (2002) to diagnose *E. granti*: (1) reduced maxillary dentition restricted to the anterior maxilla; (2) large antorbital fenestra, in a deep antorbital fossa delimited by sharp margins; (3) sharp ridge on the lateral surface of the jugal; (4) 'otic notch' below an overhanging squamosal; (5) angular and surangular marked by a strong ridge extending from the ventral margin of the mandibular fenestra; and (6) teeth with oval cross-section without carinae. Nesbitt & Butler (2013) used three of these (1, 3, 6) to revise the diagnosis of Erpetosuchidae, while others (except perhaps 6) have shown some of these characters to be common among other erpetosuchids (Nesbitt & Butler 2013; Ezcurra *et al*. 2017; Lacerda *et al*. 2018; Nesbitt *et al*. 2018) and/or shared with other groups (e.g., character 5 is present in Erpetosuchidae + Ornithosuchidae) (Von Baczko & Desojo 2016; Ezcurra *et al*. 2017; Lacerda *et al*. 2018; Müller *et al*. 2020). For this reason, we provide a revised diagnosis of *E. granti* here.

2.1. New information on *Erpetosuchus granti* (NMS G.1992.37.1)

Erpetosuchus granti was originally described by Newton (1894) and was last redescribed by Benton & Walker (2002). Minor anatomical reinterpretations were added by Ezcurra *et al*. (2017), based largely on NMS G.1992.37.1. We agree with these descriptions, except where stated explicitly herein. In this section, we expand upon these descriptions by updating the osteology of *E. granti*, based on the first μCT scans of the taxon (referred specimen: NMS G.1992.37.1). This specimen was previously studied based only on moulds and the six visible cervical (C) vertebrae (C3–C8) (Benton & Walker 2002; see Ezcurra *et al*. 2017; Supplementary material). Our μCT scans revealed previously unseen elements including: six additional vertebrae from the cervico–dorsal transition, associated osteoderms and ribs, two complete scapulae and other parts of the shoulder girdle and an almost complete forelimb (missing the distal phalanges) (Fig. 3). The μCT scans also showed a previously unnoticed pathology in the right hand (digit I) of this individual (red arrows in Fig. 3). Based on our new diagnosis, NMS G.1992.37.1 belongs to *E. granti* on the basis of markedly elongated scapula, keeled osteoderms, paramedian osteoderms that are longer than wide with unornamented anterior lamina and identical vertebral and forelimb morphology to other specimens of the species.

2.1.1. Vertebrae. A total of six cervical and six dorsal vertebrae are preserved in life position within NMS G.1992.37.1. Of these, the cervicals are partially visible in lateral view in the previously prepared cast. Ezcurra *et al*. (2017) noticed that the posterior cervical vertebrae have well-developed trapezoidal hypapophyses projecting ventrally from the surfaces of the centra (Figs 3, 4). We confirm the presence of these prominent hypapophyses and note that they decrease in size and thickness posteriorly, disappearing a few vertebrae posterior to the cervical–dorsal transition (Fig. 4). Dorsal (D) vertebrae D1 and D2 possess anteroventrally projecting hypapophyses. In D3 and D4, the hypapophyses are replaced by a single thin central keel, but from D5 onward (in the posterior direction) the ventral surface of the centrum is smooth and transversely convex (Fig. 4).

The centra of all preserved vertebrae are rectangular in lateral view (anterior and posterior articular faces are placed at the same level), being anteroposteriorly longer than dorsoventrally tall. The ratio between the length and height of the most posterior completely preserved dorsal centrum (D5) is ~1.91 (7.0 mm/3.6 mm) (Fig. 4). The transverse width across the transverse processes is greater than the centrum length in all preserved dorsal vertebrae (Fig. 4).

The neural spines are well preserved in all vertebrae (Figs 3, 4). They are rectangular in lateral view and, therefore, more similar to those of *Tarjadia ruthae* than the fan-shaped neural spines of *Parringtonia gracilis* (although a widening of the neural spine is present in the most posterior preserved dorsal vertebra (D6) of NMS G.1992.37.1). The neural spines are constant in height along the cervical and dorsal series, but are more posteriorly displaced in the dorsals. As noted by Benton & Walker (2002), the apices of the neural spines of the cervical vertebrae are transversely expanded to form 'spine tables'; this is also the case for the anterior dorsal vertebrae. The dorsal surfaces of the spine tables are concave, with a deep pit in the centre. However, the morphology of the spine table varies across the cervical–dorsal transition. The cervical spine tables are rectangular (transversely wider than anteroposteriorly long) in dorsal view, but more posteriorly the spine tables gradually become trapezoidal (with a wider anterior margin) in D3–D5, before disappearing in D6 (Fig. 4). Similarly, the pits on the dorsal surface of the spine tables become shallower along the dorsal series and no pit is present in D6 (Fig. 4). These features may be significant because the neural spines of the caudal vertebrae of BGS GSM Elgin A lack spine tables or pits, unlike those of other erpetosuchids (e.g., *P. gracilis* and *T. ruthae*) that possess both. Unfortunately, the posterior half of the skeleton is missing in all confirmed specimens of *Erpetosuchus granti*, making it impossible to make direct comparisons with BGS GSM Elgin A.

https://doi.org/10.1017/S1755691020000109 Published online by Cambridge University Press

Both the cervical and dorsal series of NMS G.1992.37.1 are associated with two rows of parasagittal osteoderms, as in the holotype (NHMUK PV R3139) (Figs 3, 4). However, this is the first time that the lateral series of osteoderms in NMS G.1992.37.1 has been revealed: the μCT scans show that they are still completely embedded in the matrix, and, thus, they were not visible in the physical moulds of the specimen (Figs 3, 4).

2.1.2. Scapula. The shoulder girdle of *E. granti* is reasonably well preserved in the holotype (NHMUK PV R3139), so little additional information can be added to the description of Benton & Walker (2002). Both scapulae are preserved in life position in NMS G.1992.37.1 and are larger than those of the holotype (37 mm in maximum length in NMS G.1992.37.1 versus 33 mm in NHMUK PV R3139), indicating that the NMS individual was marginally larger than the holotype (Fig. 3). The completeness of the scapulae of NMS G.1992.37.1 allows a more precise quantification of the proportions of this element. Uniquely within Erpetosuchidae, the scapula of *E. granti* is extremely elongated, with a total length/anteroposterior width >13 (character (Ch.) 387: 1→2). This is greater than in other relatively gracile taxa such as *P. gracilis*, where the ratio is ~8–11 (Nesbitt & Butler 2013).

2.1.3. Humerus. Both humeri of NHMUK PV R3139 have incomplete distal ends, but were each estimated to be 38 mm long (Benton & Walker 2002). The humeri in NMS G.1992.37.1 are preserved in articulation with the pectoral girdle, and whereas only the mould of the proximal third of the left humerus is preserved in the block, the entire right humerus (46.5 mm in length) is visible in the μCT scans (Figs 3, 4). The distal end is narrow transversely, reaching ~20% of the total humeral length. In addition to the description of Benton & Walker (2002), we report that the deltopectoral crest of both specimens is well developed (extends to ~1/3 of the total humeral length). No entepicondylar foramen or supinator process is visible at the distal end of the humerus, but the condyles are separated by a clear trochlear groove. A deeply excavated, long groove is visible on the posterior surface of the distal end and extends for ~1/3 of total humeral length (Fig. 3).

2.1.4. Ulna. The ulna and radius of the holotype of *E. granti* (NHMUK PV R3139) are missing their proximal ends, whereas they are completely preserved, in life position with the rest of the right forelimb, in NMS G.1992.37.1 (Fig. 3). The ulna of NMS G.1992.37.1 is long and gracile, weakly flattened and only slightly shorter than the humerus (37 mm in length excluding the olecranon process, 40 mm with this process included, against 46.5 mm, respectively). The proximal half of the ulna exhibits a weak curvature that gives the bone a sigmoidal outline in anterior and posterior views (Fig 3D, E) (not straight, *contra* Benton & Walker 2002). Its proximal end bears a prominent olecranon process that is completely fused with the shaft and a weakly developed lateral (radial) tuber (Fig. 3), just above a concave articular surface for the radius.

2.1.5. Radius. The radius of NMS G.1992.37.1 is also completely preserved, allowing for a more precise assessment of its proportions, and comparison with the humerus and ulna. The radius is subequal in length to the ulna (36.2 mm versus 37 mm excluding the olecranon process, 40 mm with this process included). The radius has a narrow shaft and proximal end that is more expanded than the distal one (Fig. 3).

2.1.6. Manus. The manus of *E. granti* is very well preserved in the holotype and has been described thoroughly (Benton & Walker 2002). To this description we add that the ratio of metacarpal distal width and length is ~0.27 (2.5 mm/7.35 mm in metacarpal I), and that we could not identify extensor pits on any of the distal ends of the metacarpals. Although the manus of NMS G.1992.37.1 is not as complete as that of NHMUK PV R3139, it is notable because of a rarely seen pathology (Fig. 3). Specifically, NMS G.1992.37.1 exhibits polydactyly, with a manus possessing six metacarpals, where 'metacarpal I' is composed of two fused metacarpals. The same pathology seems to also affect the first phalanx (Fig. 3F).

2.2. New information on *Erpetosuchus* sp. (AMNH 29300)

AMNH 29300, from the New Haven Formation of Connecticut (Hartford Basin, Newark Supergroup) of the USA, is the only specimen outside the LSF to be referred to *Erpetosuchus*. In general, we agree with the previous descriptions of this material by Olsen *et al*. (2001), and we use this section to update the anatomical description of this specimen based on examination of our CT scans, which, for the first time, allowed access to the medial side of the skull (the whole skull is exposed in left lateral view). This exercise allowed us to update scores for 20 new character states for this specimen in our phylogenetic analysis (see Supplementary material).

AMNH 29300 should still be referred to *Erpetosuchus* sp. based on the small size, and the extremely elongated posterior process of the jugal (Fig. 5) (Ch. 100–2) with an anteroposterior length/dorsoventral thickness ratio (measured at the base of the process) >~4, which is higher than in all other erpetosuchids (e.g., it scores '1' = 1.57–3.77 in *Tarjadia ruthae*; Ezcurra *et al*. 2017). AMNH 29300 may also differ from *Erpetosuchus granti* in having a maxilla that reaches as far as the anterior orbital border (Fig. 5), whereas it reaches between the posterior and anterior orbital border in *E. granti* and all other erpetosuchids. However, this region of the skull is damaged in AMNH 29300, so we were not able to score this character confidently. Because of this difference, and a lack of overlap in other diagnostic features, we cannot refer AMNH 29300 to *E. granti*, but only to *Erpetosuchus* sp.

2.2.1. Maxilla. The maxilla of AMNH 29300 has been thoroughly described and we can add little detail to the Olsen *et al*. (2001) description. Its medial side is mounted against a support. Unfortunately, the maxilla is incomplete and broken across the medial side of the alveoli. Based on the hidden alveolar margins, we can confirm the presence of ~7/8 teeth sitting in sockets and not fused to the maxilla. The antorbital fossa frames the anterior and ventral borders of the antorbital fenestra as it also does in *E. granti* and other erpetosuchids. The ventral margin of the fossa is a sharp ridge/shelf, which is highly vascularised and pierced by several foramina, as also seen in *Tarjadia ruthae* (Ezcurra *et al*. 2017) and *Parringtonia gracilis* (NMT RB28). There is no evidence for a secondary antorbital fenestra (Fig. 5), which is seen in some erythrosuchids (i.e., *Guchengosuchus shiguaiensis*, *Shansisuchus* and *Chalishevia cothurnata*; Ezcurra 2016; Butler *et al*. 2019b). The contact of the maxilla with the jugal is unclear due to a fracture running across the relevant area.

2.2.2. Jugal. As observed by Olsen *et al*. (2001), the jugal of AMNH 29300 is almost identical to that of *E. granti*. The posterior process, although broken at its base, has a distinct lateroventral orientation with respect to the anterposterior axis of the skull. This process lies distinctly ventral to the quadratojugal and extends posteriorly to nearly reach the quadrate condyles, as observed in some erpetosuchids and ornithosuchids (e.g., *E. granti*, BGS GSM Elgin A; Fig. 5) (see Von Baczko & Desojo 2016; Ezcurra *et al*. 2017; Lacerda *et al*. 2018). This process extends posteriorly beyond the occipital border of the lower temporal fenestra. The medial side of the jugal shows pneumatic structures – specifically, a series of hollow cavities and trabeculae (Fig. 5I, J). The jugal of AMNH 29300 is in close association with a very well preserved ectopterygoid, which articulates along most of the length of the medioventral edge of the orbital margin (Fig. 5).

2.2.3. Ectopterygoid. The ectopterygoid of AMNH 29300 is completely concealed in the matrix surrounding the specimen.

https://doi.org/10.1017/S1755691020000109 Published online by Cambridge University Press

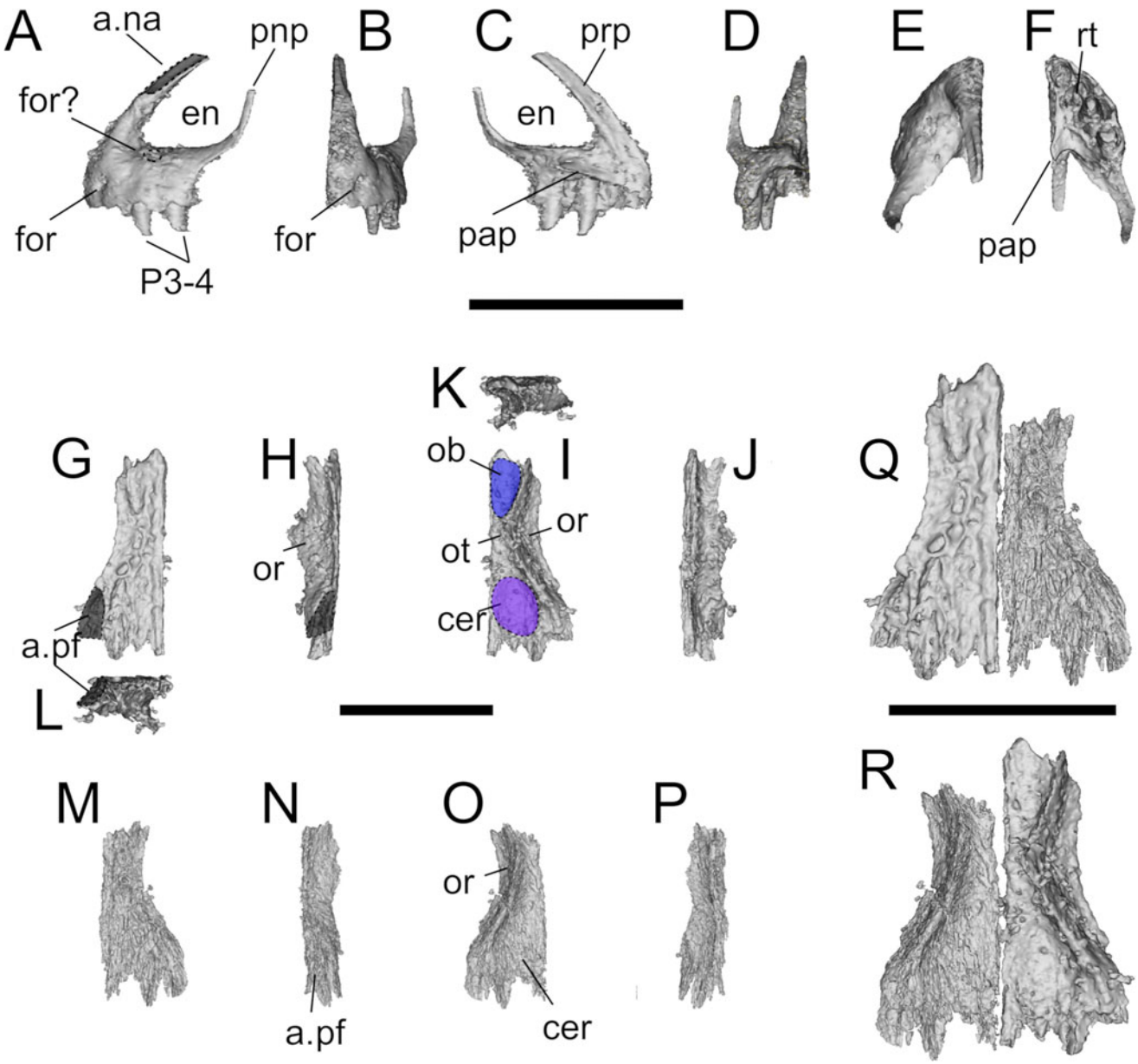

Figure 6 Erpetosuchidae indet., BGS GSM Elgin A, premaxilla and frontals. (A–F) Left premaxilla in (A) anterior, (C) medial, (D) posterior, (E) dorsal and (F) ventral views; (G–L) left frontal in (G) dorsal, (H) lateral, (I) ventral, (J) medial, (K) anterior and (L) posterior views; (M–P) right frontal in (M) dorsal, (N) lateral, (O) ventral and (P) medial views; (Q–R) articulated frontal in (Q) dorsal and (R) ventral views. Abbreviations: a.na = articulation for the nasal; a.pf = articulation for the postfrontal; cer = cerebrum; en = external nares; for = foramen; ob = olfactory bulb; or = orbit; P1-4 = premaxillary tooth 1-4; pap = palatal process; pnp = postnasal process; prp = prenasal process; rt = replacement tooth. Scale bars = 10 mm.

The main body is anterodorsally curved (much more so than in BGS GSM Elgin A) and broken (but closely associated) with a well-developed, trapezoidal posterior expansion that extends posteriorly to the base of the jugal posterior process (Fig. 5). The anterior process is intact and, as in BGS GSM Elgin A, is short and peg-like (Fig. 5E, F). In AMNH 29300, this process does not reach the maxilla.

2.2.4. Quadratojugal. The quadratojugal is very similar in morphology to that of BGS GSM Elgin A, and is still in articulation with the quadrate and closely associated with the posterior process of the jugal. The posteromedial extent of the quadratojugal overlaps the lateral side of the quadrate and does not reach the ventral condyles of the quadrate. The occipital surface of the quadratojugal of AMNH 29300 is not perforated by a foramen, unlike that of BGS GSM Elgin A (Fig. 5G, H).

2.2.5. Lower jaw. Only the posterior half of the mandible is preserved in AMNH 29300 and most of its dorsal side is hidden by the jugal. However, once the skull and matrix are digitally removed, the details of its dorsal and medial sides become available. As in other erpetosuchids, ornithosuchids and proterochampsids, the lower jaw has a strongly developed surangular shelf (Trotteyn *et al*. 2013; Ezcurra 2016; Von Baczko & Ezcurra 2016; Ezcurra *et al*. 2017). The mandibular fenestra is not completely preserved, but most of its dorsal side is intact and shows it was long compared to the overall lower jaw length. The dorsal margin of the surangular is straight. The angular is widely exposed in lateral view and not fused with the prearticular, which is also separated from the articular. The articular is pierced by a foramen on the medial side and has a medioventrally directed process. The retroarticular process is well developed and extends directly posterior to the glenoid fossa (Fig. 5).

Archosauria Cope, 1869, *sensu* Gauthier & Padian 1985
Pseudosuchia Zittel, 1887–1890, *sensu* Sereno *et al*. 2005
Suchia Krebs, 1974, *sensu* Nesbitt 2011
Erpetosuchidae Watson, 1917, *sensu* Nesbitt & Butler 2013
Erpetosuchidae gen. et sp. indet.

https://doi.org/10.1017/S1755691020000109 Published online by Cambridge University Press

Referred material. The disarticulated skeleton of BGS GSM Elgin A is embedded in BGS GSM 91072–81, 91085–6 (Figs 1, 2, 6–14). It consists of the following: left premaxilla, frontals, left lacrimal, right quadrate, left quadratojugal, right posterior lower jaw (articular, angular, surangular and associated fragments), ectopterygoid, ?pterygoid (two fragments), ?radius, fragments of dorsal vertebrae and associated osteoderm series, incomplete dorsal ribs, articulated series of middle–distal caudal vertebrae with intact osteoderms, parts of both femora (a short fragment of the shaft of the right, and the complete left), left tibia, left fibula, proximal portion of the ?pubis and three left metatarsals (two preserved as moulds). All of these elements are embedded in ten small blocks of sandstone (Figs 1, 2).

Locality and horizon. BGS GSM 91072–82, 91085–6 was collected at Spynie Quarries (NJ 223657), near to Elgin (Moray, Scotland, UK). The aeolian sandstones exposed in the quarry belong to the LSF (Upper Triassic: ~upper Carnian/lower Norian; but see Benton & Walker 2011).

2.3. Description of BGS GSM Elgin A

2.3.1. Skull. Many of the skull bones are largely complete and three-dimensionally preserved. The cranial remains are disarticulated, but closely associated in five blocks (BGS GSM 91074–8) (Figs 1, 2, 6–9). The maxilla, nasal, jugal, prefrontal, most of the palate and the braincase are missing.

Premaxilla. The left premaxilla is nearly completely preserved within BGS GSM 91076 (Fig. 6A–F). It is <10 mm long in lateral view and 5 mm wide in anterior view. In lateral view, the main body of the premaxilla is horizontally oriented (not downturned), has a rectangular shape (proportions: ~1.5 longer anteroposteriorly than deep dorsoventrally) and possesses two thin processes arising from its anterodorsal and posterodorsal margins (Fig. 6A).

The lateral surface of the main body of the premaxilla is pierced by a comparatively large (relative to the size of the premaxilla) foramen, positioned a short distance above the alveolar margin between the first and second premaxillary alveoli (P1 and P2) (Fig. 6A). This feature is shared with *Parringtonia gracilis* (NMT RB28), and potentially also other erpetosuchids (see Discussion). The μCT scans reveal that this foramen opens into a channel that extends through the premaxilla, trending dorsoventrally and exiting the bone within the external naris, along the posterior side of the base of the anterodorsal process. A proportionately smaller foramen ('anterior premaxillary foramen') can be found in the narial fossae of some early dinosaurs such as *Eoraptor lunensis* (Sereno *et al*. 1993, 2013) and *Buriolestes* (Cabreira *et al*. 2016). An additional opening, which superficially appears to be a large foramen (Fig. 6A: for?), is present on the ventral margin of the external nares, but it likely is an artefact of preservation, unlike the genuine foramen present in the 'rauisuchian' pseudosuchian archosaur *Vivaron haydeni* (Lessner *et al*. 2016).

The premaxilla bears four alveoli, but only two erupted teeth are present. These are set in sockets and the bases are not cemented to the alveolar margin (i.e., thecodont implantation: Fig. 6C, F). The four alveoli occupy the entire ventral margin of the premaxilla (Fig. 6F). There is neither an edentulous anterior margin nor a posterior subnarial diastema, which are present in aetosaurs (*Stagonolepis*, *Neoaetosauroides*, *Desmatosuchus*) and Ornithosuchidae, respectively (Desojo *et al*. 2013; Von Bazcko & Ezcurra 2013). Unfortunately, due to the small size of the specimen, few details of the dentition are available, but the teeth are weakly compressed mediolaterally, ventrally directed and are weakly recurved towards their apices; it is not clear if they have serrations. The μCT scans show a small replacement tooth medial to P2 (Fig. 6F). A small, dorsoventrally compressed palatal process projects medially and posteriorly, dorsal to alveoli P3–P4. Its posterior border is concave (Fig. 6C, F). It is unclear whether interdental plates were present on the medial side of the premaxilla.

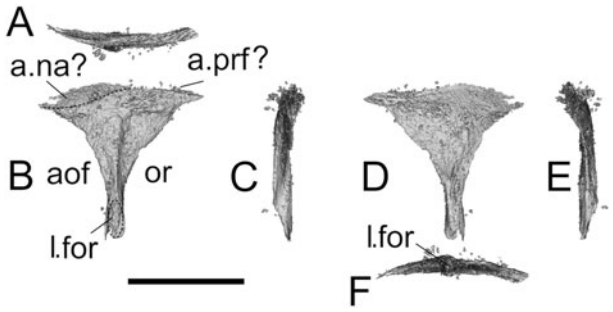

Figure 7 Erpetosuchidae indet., BGS GSM Elgin A, right lacrimal. (A–F) Lacrimal in (A) dorsal, (B) lateral, (C) anterior, (D) medial, (E) posterior and (F) ventral views. Abbreviations: a.mx = articulation for the maxilla; a.na = articulation for the nasal; aof = antorbital fenestra; a.prf = articulation for the prefrontal; l.for = lacrimal foramen; or = orbit. Scale bars = 10 mm.

The anterior margin of the main body of the premaxilla is subvertical in lateral view (Fig. 6A). Above it, the thin, elongate anterior process (= nasal process) extends posterodorsally at ~60° to the horizontal in lateral view (Fig. 6A, C). This process (measured from base of external nares to its posterior end) is shorter than the anteroposterior length of the premaxilla and forms the anterior and dorsal margins of the external nares. Its lateral surface bears an unusually long, slot-like articular surface for the nasal (Fig. 6A); the anterior extent of this surface indicates that the nasal would have participated in the anterodorsal margin of the external nares. The shape and orientation of this slot indicates that the nasals were separated from each other anteriorly by thin processes of the premaxillae that met along the midline. Finally, as is common in archosaurs, the relative positions of the nasal articulation and the posterior border of the main body of the premaxilla indicate that the nasal reached further anteriorly than the maxilla in lateral view (Fig. 6A, E).

The posterodorsal (= maxillary or subnarial process) process is thinner in lateral and posterior views than the anterior process (Fig. 6A, C). The posterodorsal process initially projects posteriorly at a low angle (~30°) before bending sharply dorsally to become sub-vertical. This morphology is unusual and creates a distinctive 'step-like' contact between the premaxilla and maxilla that is, to our knowledge, unique within Pseudosuchia (Nesbitt 2011; Ezcurra 2016; Roberto-da-Silva *et al*. 2016), and which is similar to the condition in the early dinosaur *Eoraptor lunensis* (see Sereno *et al*. 1993, 2013). However, this part of the posterodorsal process is often broken in many specimens. The posterodorsal process forms the posterior margin of the external naris and excluded the maxilla from participating in the border of this opening (Fig. 6A). The exclusion of the maxilla from the border of the external naris is plesiomorphic in Archosauriformes and the maxilla participates in the border only in a small number of taxa (e.g., all aetosaurs except *Aetosauroides*, *Batrachotomus kupferzellensis*, *Effigia*, *Arizonasaurus*) (Gower 1999; Nesbitt 2011; Desojo *et al*. 2013).

The external nares are positioned at the anterior end of the snout, open laterally and are triangular in lateral view (this is a potential autapomorphy of BGS GSM Elgin A within Erpetosuchidae) (Fig. 6A); by contrast, they are normally circular or oval in other archosaurs. The ventral, anterodorsal and posterior margins of the external naris are formed, respectively, by the premaxilla main body, premaxillary anterior process and nasal, and premaxillary posterodorsal process. There is no evidence of either a substantial narial fossa or a subnarial fenestra between the premaxilla and maxilla (Fig. 6A). The subnarial fossa is

https://doi.org/10.1017/S1755691020000109 Published online by Cambridge University Press

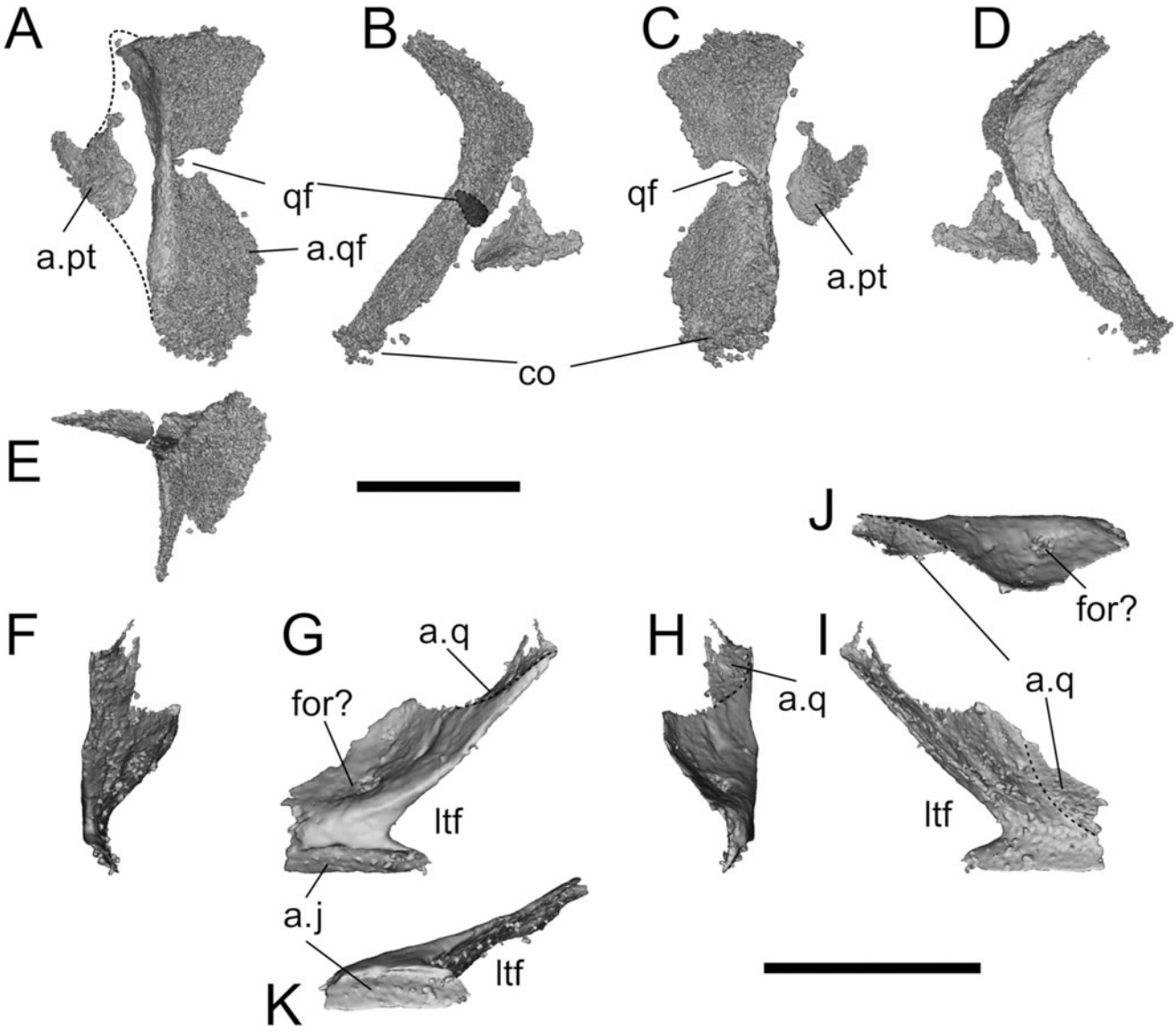

Figure 8 Erpetosuchidae indet., BGS GSM Elgin A, quadrate and quadratojugal. (A–E) Quadrate in (A) posterodorsal, (B) lateral, (C) anteroventral, (D) medial and (E) ventral views; (F–K) quadratojugal in (F) anterior, (G) lateral, (H) posterior, (I) medial, (J) dorsal and (K) ventral views. Abbreviations: a.co = articular condyles; a.j = articulation for the jugal; a.pt = articulation for the pterygoid; a.q = articulation for the quadrate; a.qj = articulation for the quadratojugal; a.sq = articulation for the squamosal; for = foramen; ltf = lower temporal fenestra qf = quadrate foramen. Scale bars = 10 mm.

commonly found in dinosaurs such as *Eoraptor*, *Herrerasaurus*, sauropodomorphs and theropods (Nesbitt 2011), but only rarely in pseudosuchians (e.g., *B. kupferzellensis*: Gower 1999).

Frontal. Both frontals of BGS GSM Elgin A are well preserved and easily identifiable in BGS GSM 91077 (left) and BGS GSM 91075 (right) (Fig. 6G–P). The right frontal (Fig. 6G–I) is nearly complete and ~15 mm long anteroposteriorly, whereas the left element is missing its anterior tip (Fig. 6M–P). The frontals are separate (i.e., unfused along the midline) and are longer than wide. Their dorsal surfaces are densely sculptured by a random (non-radial) pattern of ridges and grooves similar to those of early suchians (e.g., *Gracilisuchus* – MCZ 4117; *Parringtonia* – Nesbitt *et al*. 2018), and lack any distinguishable ridge or fossa near the midline (Fig. 6H, N), in contrast to the presence of these features in *Batrachotomus*, *Postosuchus* and some crocodylomorphs (e.g., *Dromicosuchus*, *Hesperosuchus*, *Sphenosuchus*; Clark *et al*. 2000; Sues *et al*. 2003; Nesbitt 2011), which are characterised by a distinct midline fossa. The orbital margin of the frontal is slightly raised relative to the rest of the dorsal surface. The frontal is as transversely wide along its anterior portion as it is medial to the orbital margin, as in most archosauriforms (e.g., ornithosuchids, phytosaurs, aetosaurs, gracilisuchids: Walker 1964; Nesbitt 2011; Desojo *et al*. 2013; Stocker & Butler 2013; Butler *et al*. 2014). However, the frontal expands laterally posterior to the narrowest interorbital distance, such that the posterior end is nearly twice the width of the anterior end (Fig. 6H, N). This gives the combined frontals a trapezoidal outline in dorsal view (Fig. 6Q–R).

The anterior suture with the nasal is such that the frontals would have projected a short distance between the nasals, whereas the posterior margins of both frontals form an interdigitated ('W'-shaped) suture with the parietals (Fig. 6G, M). Along its posteromedial margin there is no evidence that the frontal participated in the supratemporal fenestra. Absence of frontal participation in the supratemporal fenestra is the condition in most Triassic archosaurs (Ezcurra 2016). In lateral view, the frontal forms the entire dorsal margin of the orbit (Fig. 6G–P). The posterolateral corner of each frontal has a depression that likely represents the articulation surface for either the postfrontal or postorbital (if the postfrontal was absent) (Fig. 6G, H, I). The ventral surfaces of the frontals have distinct fossae that represent the impressions of the olfactory bulbs (Fig. 6I, O). These are linked to fossae that represent the impressions of the rest of the cerebrum by the hourglass-shaped impressions of

https://doi.org/10.1017/S1755691020000109 Published online by Cambridge University Press

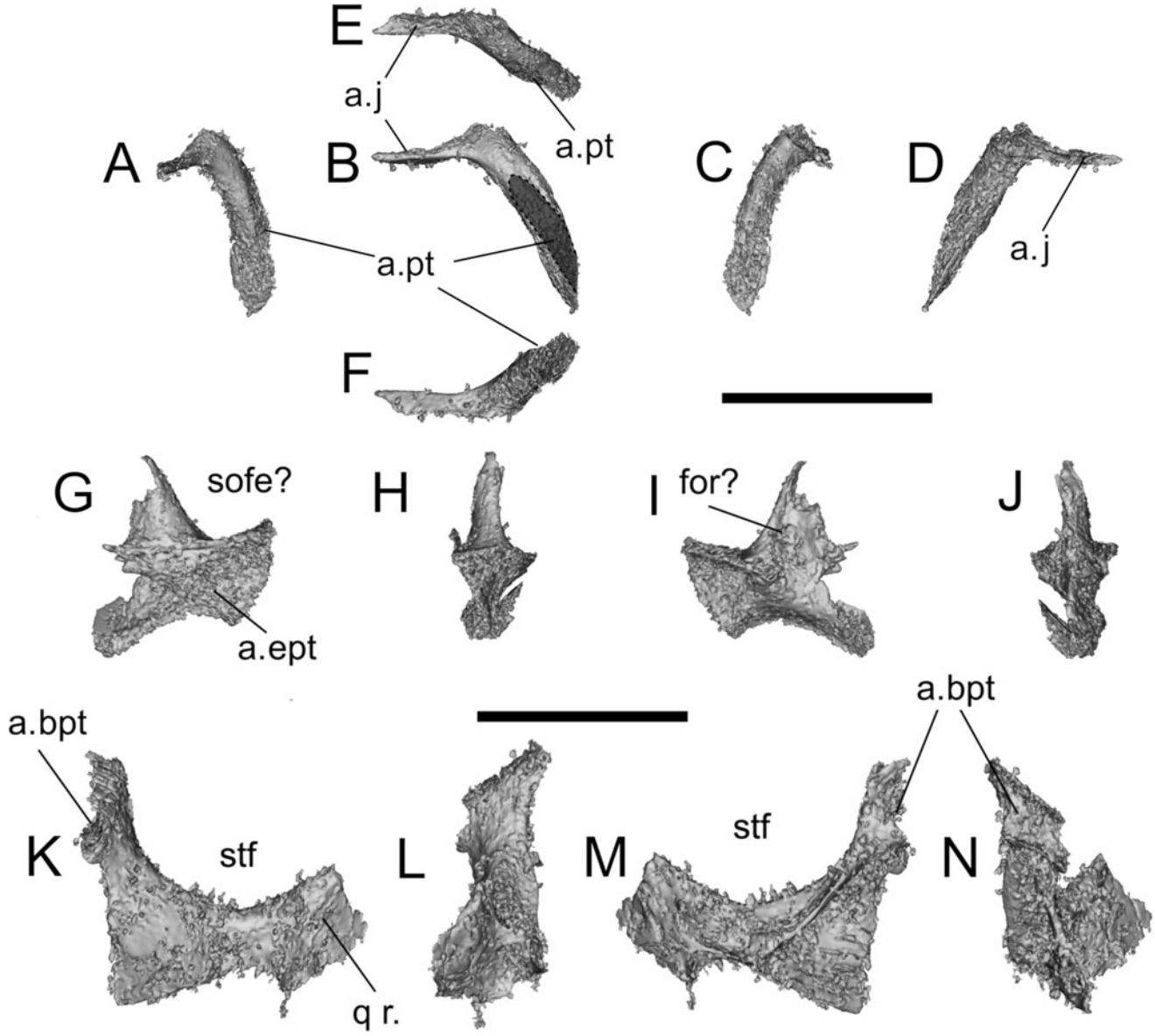

Figure 9 Erpetosuchidae indet., BGS GSM Elgin A, left ectopterygoid and two pterygoid fragments. (A–F) Ectopterygoid in (A) anterior, (B) lateral, (C) posterior, (D) medial, (E) dorsal and (F) ventral views; (G–J) middle-left section of the pterygoid; (K–N) posterior portion of the left pterygoid. Abbreviations: a.bpt = articulation for the basipterygoid; a.ept = articulation for the ectopterygoid; a.j = articulation for the jugal; a.pt = articulation for the pterygoid; a.qj = articulation for the quadratojugal; q r. = quadrate ramus of the pterygoid; sofe = suborbital fenestra; stf = subtemporal fenestra. Scale bars = 10 mm.

the olfactory tracts. The crista cranii that separate the orbits from these endocranial structures are well-developed tall ridges.

Lacrimal. The right lacrimal is completely embedded within BGS GSM 91078 (Fig. 7), has a triangular outline in lateral view and is flat and slightly concave medially. One of the extremities, here interpreted as the ventral process, is tubular in cross-section with a low crest extending along the lateral surface and would presumably have articulated with the anterodorsal process of the jugal. This process terminates ventrally in a large foramen that is similar to, but more ventrally placed than, that reported on the lacrimal of the pseudosuchian *Prestosuchus chiniquensis* (Mastrantonio *et al*. 2019). This foramen opens into a canal that extends through the bone and that emerges medially at the dorsal end of the ventral process (Fig. 7B, D, F). The shape of the lacrimal of BGS GSM Elgin A is unusual, in that the posterior prefrontal process is more prominent than in most known archosaurs BGS GSM Elgin A. A shallow fossa is present on the anterior process that is interpreted as part of the antorbital fossa. The gently curved posterior margin forms the anterior edge of the orbit. Sulci and flat articular surfaces, probably for the nasal and prefrontal, are visible on the anterior and posterior processes in lateral and dorsal views (Fig. 7B: a.na, a.prf?).

Quadrate. The right quadrate is nearly completely preserved, although its main body (in BGS GSM 91076) has been separated from the medial pterygoid process (in BGS GSM 91079) (Fig. 8A–E). The articular condyles and the anterior extremity of the pterygoid process are not as well preserved, although it is unclear whether this is due to poor ossification, diagenetic damage or both. A large foramen, interpreted as the quadrate foramen (Fig. 8A–C: qf), is visible on the lateral surface near the quadrate-quadratojugal articulation – this feature is present in all non-archosaurian archosauromorphs, and many crown archosaurs, but absent in crocodylomorphs (Nesbitt 2011). Neither the anterior nor posterior surfaces of the quadrate bear significant grooves or crests. The dorsal portion of the quadrate is triangular in dorsal view, with a prominent dorsal and posteriorly directed process.

Quadratojugal. The right quadratojugal of BGS GSM Elgin A is preserved in BGS GSM 91077 in close association with a fragment of the lower jaw (Fig. 8F–K). In lateral view, this bone has a

https://doi.org/10.1017/S1755691020000109 Published online by Cambridge University Press

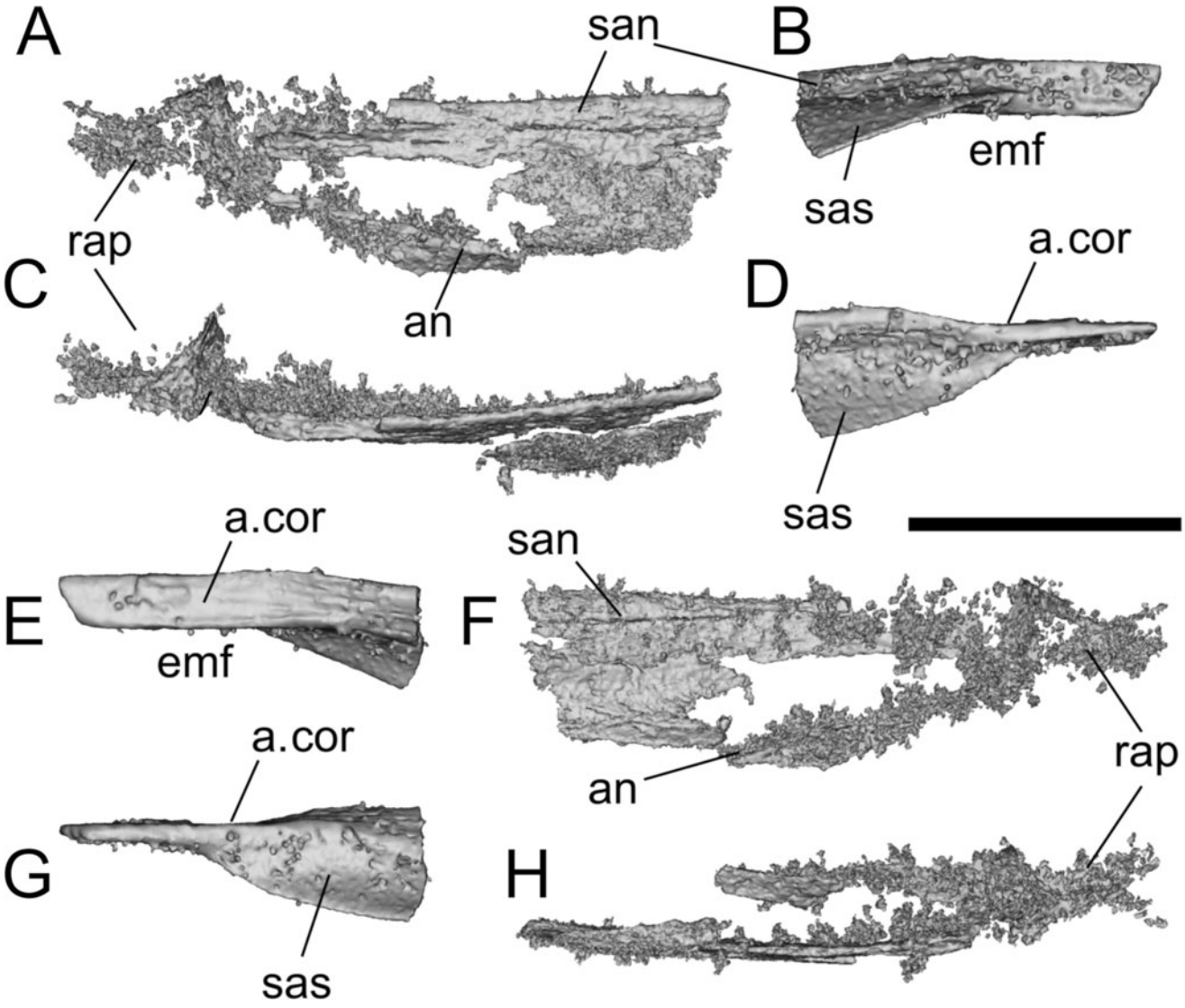

Figure 10 Erpetosuchidae indet., BGS GSM Elgin A, posterior right lower jaw fragments in (A, B) lateral, (C, D) dorsal, (E, F) medial and (G, H) ventral views. Abbreviations: a.cor = articulation for the coronoid; an = angular; emf = external mandibular fenestra; rap = retroarticular process; san = surangular; sas = surangular shelf. Scale bar = 10 mm.

characteristic 'L'-shaped outline (Fig. 8G). The angle between the anterior and dorsal processes is acute (~40°), a feature shared by Ornithosuchidae and Erpetosuchidae within Pseudosuchia (Von Baczko & Desojo 2016; Ezcurra *et al*. 2017; Lacerda *et al*. 2018; but see Discussion). The main body of the quadratojugal is an arched thin sheet that in life wrapped around the lateral surface of the quadrate and contacted the posterior process of the jugal ventrally. The anterior surface of the quadratojugal is concave and formed the posterior and ventral walls of the lower temporal fenestra. The posterior surface is also smooth and concave, and pierced by a foramen, which is not seen in other archosaurs (Fig. 8G, J: for?; see Discussion).

The articular surfaces for the posterior process of the jugal and the quadrate are both visible (Fig. 8G–K: a.q, a.j). The first is positioned on the ventral surface of the bone, indicating that in life the jugal would articulate on the ventral surface of the anterior process of the quadratojugal, and that the jugal posterior process extended far posteriorly, reaching close to the quadrate condyles. The first character state is shared with crocodylomorphs (e.g., *Dromicosuchus*), *Postosuchus kirkpatricki*, *Polonosuchus* and *Gracilisuchus* (Chatterjee 1985; Sues *et al*. 2003; Nesbitt 2011; Weinbaum 2011) among pseudosuchians. The latter character state (i.e., the jugal posterior process extending as far as the quadrate condyles) is shared with erpetosuchids, most phytosaurs, crocodylomorphs (Benton & Walker 2002; Nesbitt 2011; Ezcurra *et al*. 2017; Stocker *et al*. 2017) and some rauisuchians (Gower 1999; Nesbitt *et al*. 2013; but see Discussion). The articular surfaces for the quadrate on the ventral and dorsal parts of the medial surface of the quadratojugal are both well preserved (Fig. 8G, I–K).

Ectopterygoid. The right ectopterygoid is preserved in BGS GSM 91079 and is a long, weakly curved, comma-shaped element (Fig. 9A–F). The main body is elongated and bears traces of the articulation with the pterygoid on the posteromedial surface (Fig. 9A–C: a.pt). The lateral process is lost and, on the other side, a straight, rod-like process is visible (Fig. 9B–E: a.j). However, based on the preserved element, it is not possible to determine whether the ectopterygoid articulated with the maxilla, nor the extent of its lateral contact with the jugal (the ectopterygoid has an expanded contact with the jugal in *Erpetosuchus granti* and *Erpetosuchus* sp. (AMNH 29300)) (Fig. 5) (Olsen *et al*. 2001; Benton & Walker 2002).

The ectopterygoid has a single head, as opposed to the 'rauisuchians' *Postosuchus*, *Polonosuchus* and *Batrachotomus*, in which a double head is present (Chatterjee 1985; Gower 1999; Nesbitt 2011; Weinbaum 2011; Nesbitt *et al*. 2013). The ectopterygoid arches anteriorly in dorsal view and maintains a subcircular to sub-triangular cross-section along most of its length

https://doi.org/10.1017/S1755691020000109 Published online by Cambridge University Press

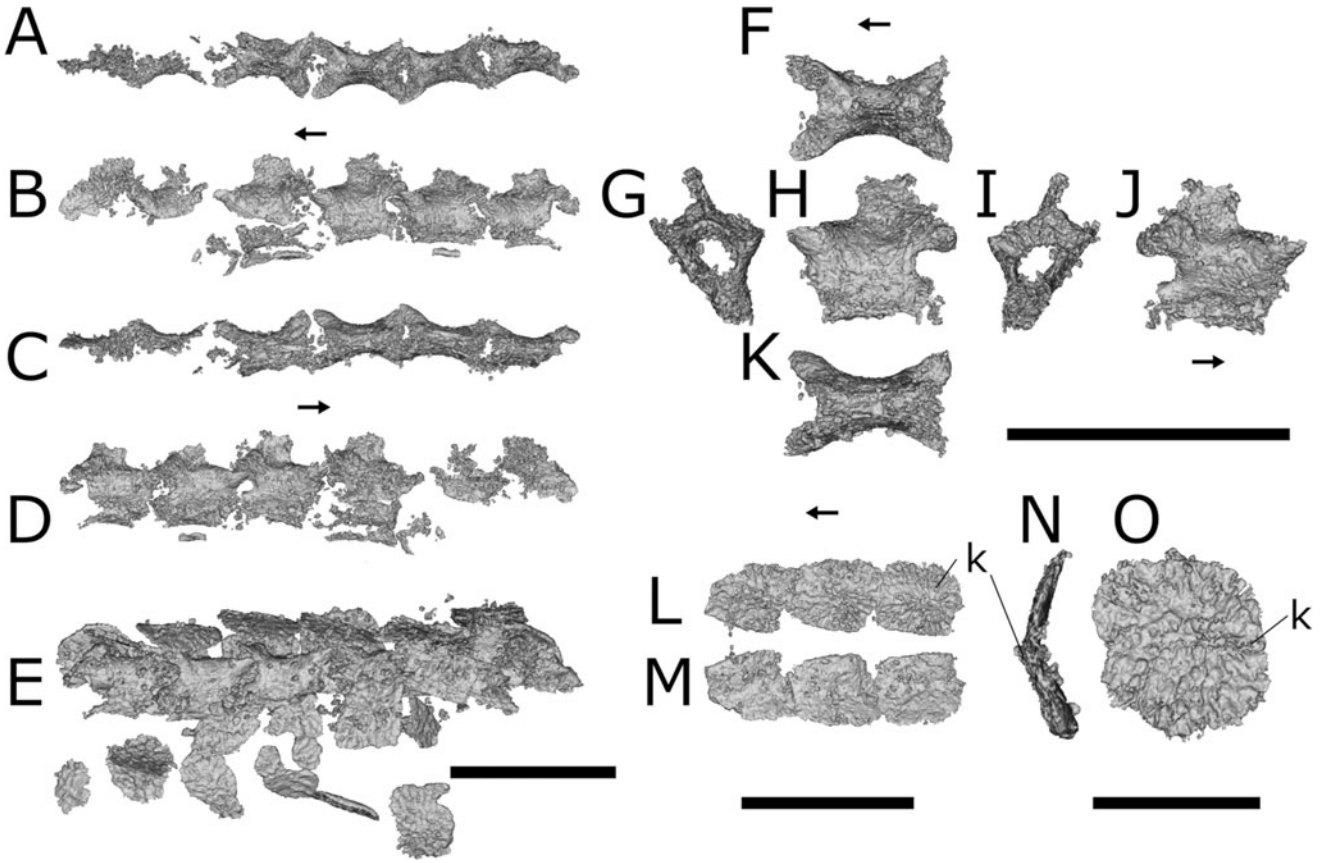

Figure 11 Erpetosuchidae indet., BGS GSM Elgin A, articulated middle–posterior series of caudal vertebrae, caudal vertebra and osteoderms. (A–E) Series of middle-posterior caudal vertebrae in (A) dorsal, (B) left lateral, (C) ventral and (D, E) right lateral views (E with associated osteoderms); (F–K) caudal vertebra in (F) dorsal, (G) anterior, (H) left lateral, (I) posterior, (J) right lateral and (K) ventral views; (L, M) paramedian row of caudal osteoderms in (L) dorsal and (M) ventral views; (N, O) close-up of caudal paramedian osteoderm in (N) anterior and (O) dorsal views. Abbreviation: k = keel. Scale bars = 10 mm (E, I, J, L, M); 5 mm (N, O).

before it tapers and flares laterally at its distal end. In contrast to most archosaurs, the main body of the ectopterygoid is not significantly arched anteriorly or anterodorsally but is mostly straight as in *Revueltosaurus* (Parker *et al*. 2005). The posteromedial surface of the bone shows an articular surface for the lateral and ventral parts of the pterygoid.

Pterygoid. Two fragments preserved in BGS GSM 91076 are here interpreted as parts of the pterygoids (Fig. 9G–N). We interpret the first as the lateral part of the right pterygoid (preserving an articular facet for the ectopterygoid) (Fig. 9G–J). The second fragment (Fig. 9K–N) is identified as the posterior portion of the left pterygoid, preserving the medial margin of the subtemporal fenestra, part of the basipterygoid articulation and the damaged base of the quadrate ramus (Fig. 9K: q r.). A complex system of thin crests is visible on one side of the bone. There is no evidence of teeth on either of the preserved pterygoid fragments.

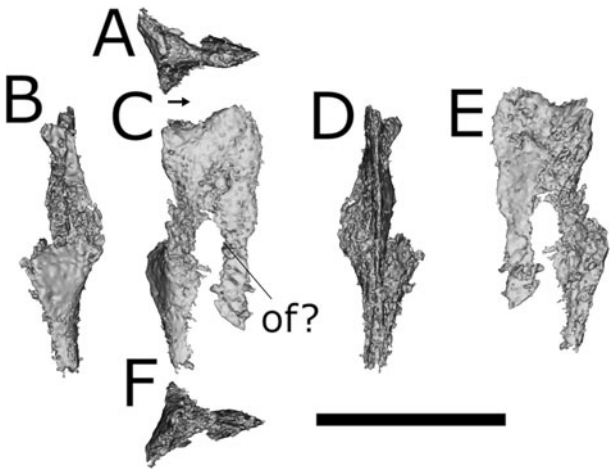

Figure 12 Erpetosuchidae indet., BGS GSM Elgin A, pubis? in (A) dorsal, (B) posterior, (C) lateral, (D) anterior, (E) medial and (F) ventral views. Abbreviation: of = obturator foramen. Scale bar = 10 mm.

2.3.2. Lower jaw. The posterior part of the right lower jaw is preserved in BGS GSM 91076 and includes parts of the posterior portion of the angular and parts of the surangular (Fig. 10). There is evidence that an external mandibular fenestra was present, but no other internal mandibular cavity could be identified due to the poor preservation. Posterior to this the angular is widely exposed on the lateral surface of the mandibular ramus. Additional useful diagnostic features cannot be assessed due to the poor preservation of the fragments.

We identified one of the associated lower jaw fragments as the anterior part of a mediolaterally broad surangular shelf. A similar wide shelf is present in *Parringtonia* (NMT RB 426), *Erpetosuchus* sp. (AMNH 29300; Fig. 5) and some other archosauriforms (see Discussion). Additional bone shards, presumably belonging to the splenial, angular and surangular, are preserved in BGS GSM 91076 and 91079 close to the other mandibular fragments (Fig. 10B, D, E, G). There is no evidence of a surangular foramen in any of these fragments.

2.3.3. Vertebral column and osteoderms. Incomplete fragments of vertebrae and associated osteoderms belonging to BGS GSM Elgin A are found in several blocks (Figs 2, 11). A

https://doi.org/10.1017/S1755691020000109 Published online by Cambridge University Press

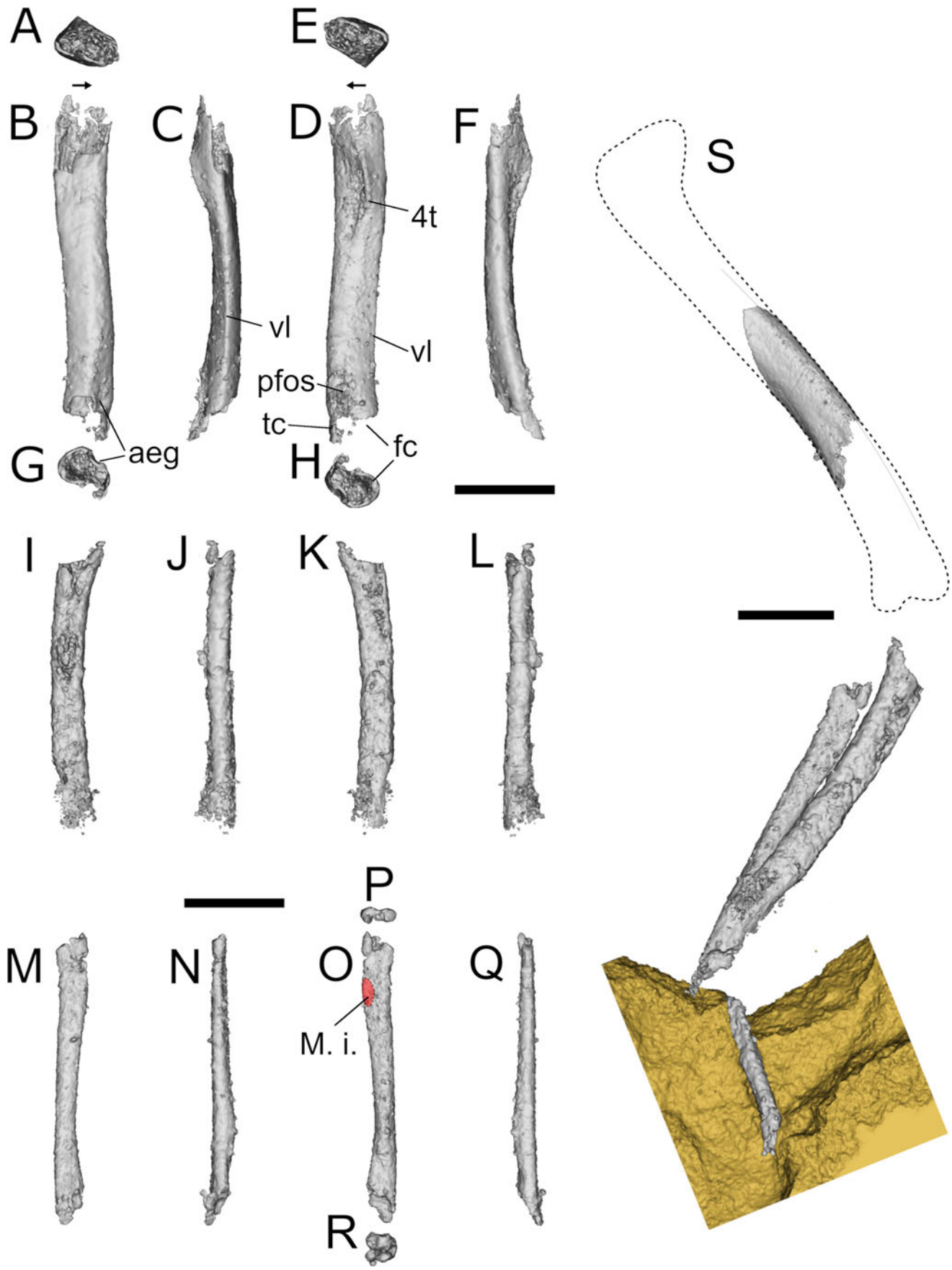

Figure 13 Erpetosuchidae indet., BGS GSM Elgin A, right femur, left tibia, left fibula and articulated partial left leg. (A, E) Right femur in proximal, (B) lateral, (C) posterior, (D) medial, (F) anterior and (G, H) distal views; (I–L) left tibia in (I) medial, (J) anterior, (K) lateral and (L) posterior views; (M–R) left fibula in (M) lateral, (N) anterior, (O) medial, (P) proximal, (Q) posterior and (R) distal views; (S) left leg in lateral view. Abbreviations: aeg = anterior extensor groove; fc = fibular condyle; 4t = fourth trochanter; M. i = attachment for the M. iliofibularis; pfos = popliteal fossa?; tc = tibial condyle; vl = ventrolateral edge. Scale bars = 10 mm.

https://doi.org/10.1017/S1755691020000109 Published online by Cambridge University Press

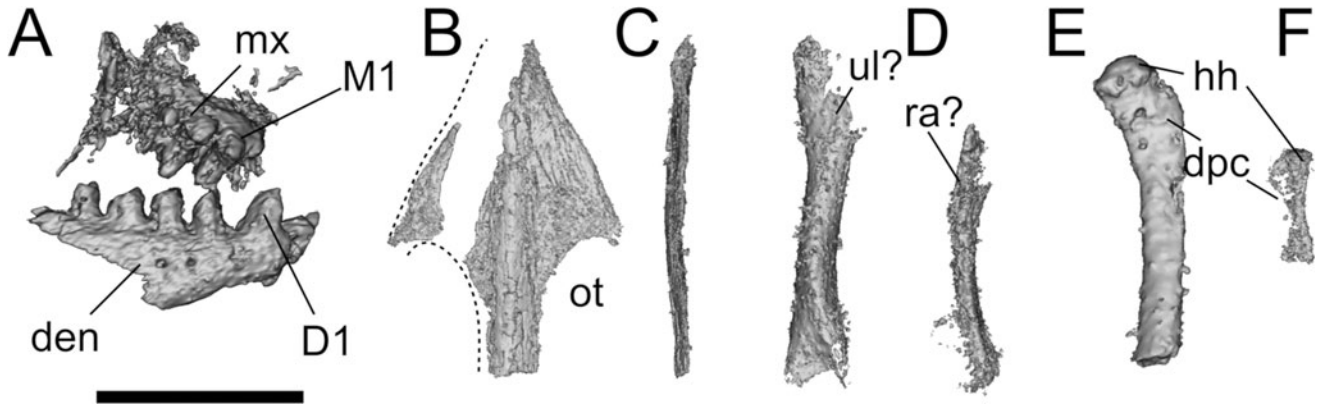

Figure 14 *Leptopleuron lacertinum* bones and indeterminate elements in BGS GSM 91072–82, 91085–6 blocks. (A) *Leptopleuron lacertinum*, BGS GSM Elgin P, right dentary and maxilla and bicuspid teeth in lateral view; (B, C) skull roof of *L. lacertinum*, BGS GSM Elgin P in (B) dorsal and (C) lateral view; (D, E) radius and ulna of indeterminate taxon in BGS GSM 91074 + 91077; (E) humerus of indeterminate taxon in BGS GSM 91078; (F) humerus of indeterminate taxon in BGS GSM 91074 + 91077. Abbreviations: den = dentary; Dn = nth dentary tooth; dpc = deltopectoral crest; hh = humeral head; Mn = nth maxillary tooth; mx = maxilla; ot = orbito-temporal fossa; ra = radius; ul = ulna Scale bar = 10 mm.

long, fragmented series of osteoderms and broken ribs can be traced along the surface of BGS GSM 91076 and continues on BGS GSM 91073–5 and GSM 91086 (Figs 1, 2). Based on their close proximity with the skull fragments, and the orientation of the rest of the skeleton, these are likely associated with the precaudal part of the vertebral series. Associated with these are a putative radius/ulna and a possible pubis fragment (Figs 1, 12).

Twelve pairs of articulated osteoderms and moulds or fragments of partial vertebrae are present in BGS GSM 91081 and 91085 (Fig. 2). This series presumably represents the posterior dorsal, sacral and anterior caudal vertebrae. Finally, an articulated series of nine distal caudal vertebrae and associated osteoderms are split between BGS GSM 91074 and 91072 (Figs 2, 11). This segment is almost certainly the continuation of the previous series, although, as previously mentioned, an unambiguous connection between the blocks BGS GSM 91072/91074 and 91085/91081 has not been recognised (see Introduction). Unfortunately, little information can be gleaned from the presacral series, but the caudal sequence is well preserved and only slightly distorted (Figs 2, 11). These middle–posterior caudals are the only vertebrae that warrant full description (Fig. 11A–K).

Vertebrae. The middle and distal caudal vertebrae are intact and only slightly distorted. This caudal series has some peculiar characteristics (Fig. 11A–K). The centra are strongly reduced in size relative to the neural arches, with the neurocentral canal being wider and taller than the centra in cross-section (Fig. 11F–K). The neural spines are rectangular and low in lateral view and lack any transverse expansion at their dorsal ends (i.e., spine tables are absent). Expansions of the apices of the neural spines are present in many pseudosuchian archosaur lineages (including Rauisuchidae, Phytosauria, Ornithosuchidae, Aetosauria and Erpetosuchidae; but see Discussion). It is noteworthy, however, that complete caudal series are rarely preserved, and the spine table character has been assessed primarily on cervical/dorsal and anterior caudal vertebrae. Spine tables are present on some caudals of *Parringtonia gracilis* (see Discussion). No accessory neural spine, haemal arch or lateral processes (caudal ribs) are present on any of these associated vertebrae, indicating that they possibly represent a segment of the middle to distal tail.

Osteoderms. Osteoderms are preserved in articulated parasagittally arranged rows within multiple blocks (BGS GSM 91081, 91085–6, 91072–4, 91077; Figs 2, 11). Each vertebra of the caudal series is associated with two rows of thin osteoderms per side (a paramedian and lateral row per side; Fig. 11E, L–O). The dorsal surface of each osteoderm is conspicuously ornamented with pits and grooves, but the ventral surface is smooth. The paramedian osteoderms are approximately square in shape (only slightly longer than wide), with a visible keel along the midline that is also the hinge of a weak mediolateral curvature (Fig. 11N–O; see Discussion). The lateral osteoderms are narrower, rectangular and their lateral edge is irregular; they are also smaller and, in contrast to the paramedian osteoderms, they are flat and lack a clear longitudinal keel (Fig. 11L–M). Successive rows of paramedian osteoderms are imbricated, with the anterior margin of each osteoderm being minimally covered by the posterior margin of the previous one. Based on the combined number of osteoderm rows and the one-to-one association with vertebrae of the caudal region, the tail would comprise at least 20 vertebrae. There is no indication of appendicular osteoderms, although, if present, they might be too small to be detected in the μCT scans.

2.3.4. Forelimb. The only trace of a possible humerus, as noted by Walker (1964), is preserved on the surface of BGS GSM 91081 and 91085, but is not clearly visible in the μCT datasets. Considering its poor state of preservation, it is not possible to comment further on its morphology.

A long and thin element, presumably the radius or ulna, is present in BGS GSM 91074 and 91077, lateral to the ribs and osteoderms. No further anatomical details are available (Fig. 2).

2.3.5. Pelvic girdle and hind limb. A putative pelvic girdle element is present at the end of the partial vertebral column segment in BGS GSM 91073–5 and 91086. Parts of both hind limbs are partially exposed in association, with a series of dorsal/caudal osteoderms, and the moulds of the centra of a few vertebrae in BGS GSM 91081. The pelvic girdle elements are so fragmentary that it is impossible to comment further on their morphology.

Pelvic girdle. A fragment of what could be the proximal end of the pubis with an obturator foramen is present in BGS GSM 91072 (Fig. 12).

Femur. Two femoral fragments are partially exposed on the surface of BGS GSM 91081 (Figs 1–2, 13). Neither is complete and both are missing the epiphyses and parts of their shafts. They are both partially exposed in lateral view. The following description is based on the right femur, which is missing only the femoral head and distal condyles (Fig. 13A–H). The femur has a weakly sigmoidal outline (Fig. 13B, D). The lateral surface of the shaft is smooth. The femur bears no trace of a trochanteric shelf (possible attachment for the M. iliofemoralis in *Erythrosuchus africanus* and in *Mandasuchus tanyauchen* amongst pseudosuchian archosaurs and dinosauriforms; Gower 2003; Nesbitt

https://doi.org/10.1017/S1755691020000109 Published online by Cambridge University Press

2011; Butler *et al.* 2018). Conversely, the attachment for the M. caudofemoralis group (= fourth trochanter) is clearly exposed on the medial (ventral) side of the femur (Fig. 13D: 4t) and trends parallel to the long axis of the bone. This crest is low, distinctly separated from the proximal head and is not associated with an intertrochanteric fossa. These latter features are similar to pseudosuchian archosaurs, which also have a mound-like and symmetrical trochanter (as also in non-archosaurian archosauriforms), as opposed to the morphologies (trochanter is absent or present as a sharp flange) present in avemetatarsalian archosaurs (Langer & Benton 2006; Nesbitt 2011; Ezcurra 2016). The femur of BGS GSM Elgin A is unusually thin-walled, with a thickness/diameter ratio of ~0.225 (Ch. 508–1), which is rare, but not unique amongst pseudosuchian archosaurs (e.g., *Effigia*, *Arizonasaurus*, *Poposaurus* and *Terrestrisuchus*; see Nesbitt 2007, 2011; Schachner *et al.* 2020) (see Discussion). Although incomplete, the preserved distal end hints that the fibular condyle had a rounded cross-section and was distinctly larger than the tibial condyle, as in most archosauriforms (Fig. 13H). A small groove, identified here as the anterior extensor groove, is present as a small concavity limited to the most distal part of the anterior surface of the bone (Fig. 13B, G).

Tibia. The tibia is closely associated with the left femur, fibula and the moulds of three metatarsals. Of the two bones associated with the femur, we identify the larger one as the tibia (Figs 2, 13I–L). The left tibia is a slender bone missing the distal and proximal ends (Fig. 14A–D). It is completely embedded in BGS GSM 91081 so that it is only revealed by µCT scans (Figs 1, 2, 13I–L). Its total preserved length (28.3 mm) makes it shorter than the preserved length of the right femur (33.6 mm), even accounting for the missing ends. The estimated length is difficult to assess, but the life position of the bones in the matrix hint that the complete femur would be longer than the complete tibia. The femur is longer than the tibia (or fibula) in non-archosaurian archosauriforms, pseudosuchian archosaurs, herrerasaurids and post-Carnian sauropodomorphs (Müller *et al.* 2018). The lateral surface of the bone is smooth and lacks a clearly defined fibular crest. The shaft is subcircular in cross-section.

Fibula. The left fibula is associated with the other bones of the left hind limb in approximate life position. It is missing the distal and proximal ends (Fig. 13M–R) but appears to have been transversely compressed. Its width at mid-length is distinctively less than that of the tibia, as in most archosauromorphs except *Tanystropheus longobardicus* (Ezcurra 2016). The attachment of the M. iliofibularis is located on the proximal third of the bone and is visible as a small flattened surface (Fig. 13O: M. I). This condition contrasts with the well-developed tubercle positioned approximately at the midshaft that is present in phytosaurs, ornithosuchids and aetosaurs (Sereno 1991; Parrish 1993; Nesbitt 2011).

Foot. The moulds of three undetermined metatarsals are preserved between BGS GSM 91081 and BGS GSM 91080, close to the distal end of tibia and fibula (Figs 2, 14K). Little can be said about them other than they are unfused, considerably shorter than both the tibia and fibula (approximate maximum length of the longest element is ~14.5 mm), and, thus, are not as elongated as those of most avemetatarsalian archosaurs (Sereno 1991; Nesbitt 2011).

2.4. BGS GSM Elgin P and indeterminate bones in BGS GSM 91072–82, 91085–6

Within the blocks of BGS GSM 91072–82, 91085–6 there are several bones that cannot be assigned to the unnamed pseudosuchian (BGS GSM Elgin A). We refrain from referring these bones to BGS GSM Elgin A due to differences in anatomical features, size, textures and location (they are scattered away from the main cluster of that skeleton). Furthermore, these bones are in some cases easily identifiable as representing another taxon.

BGS GSM 91072–81, 91085–6 contains a previously unknown specimen of the procolophonid *Leptopleuron lacertinum*. A handful of bones embedded in BGS GSM 91074–78 are identified as damaged cranial elements (dentary, partial anterior snout with teeth and a skull roof; Fig. 14A–C), ribs and other unidentifiable fragments, all belonging to the same individual (BGS GSM Elgin P). The dentary and maxilla show features diagnostic of Procolophonidae, and specifically *L. lacertinum*, which is known from the same age and locations (Säilä 2010). These features include: frontal narrow between the orbitotemporal openings; bicusped, labiolingually wide maxillary teeth (with the two cusps linked by a sharp ridge); and maxillary tooth (M2) larger than maxillary tooth 1 (M1) (Säilä 2010; Zaher *et al.* 2019) (Fig. 14).

Potentially belonging to this specimen (BGS GSM Elgin P) are two closely associated long bones (radius and ulna) in BGS GSM 91077, 91074. Unfortunately, and similar to most of the other long bones in BGS GSM 91072–81, 91085–6, the epiphyses are poorly preserved, so only limited information is available (Fig. 14D, E).

Finally, two additional bones, not belonging to either BGS GSM Elgin A or L, are tentatively identified here as humeri. The first lies within BGS GSM 91076+78, but is separate from the BGS GSM Elgin A bone cluster. Whereas this humerus is missing its distal end, its proximal end is intact, with a visible rounded head (Fig. 14E). The second putative humerus is considerably smaller, with a well-developed deltopectoral crest (Fig. 14F). These apparently underwhelming bones are not clearly referable to any of the known Elgin reptiles. This suggests that they may belong to previously unrecognised taxa in the assemblage, hinting at an underappreciated diversity in the LSF late deposits.

3. Discussion

3.1. Comparisons of BGS GSM Elgin A with other archosaurs

The µCT scans reveal a combination of features (e.g., osteoderms, femur/tibia proportions, presence of a low fourth trochanter) that indicate that BGS GSM Elgin A is a pseudosuchian archosaur (Nesbitt 2011). However, this new information falsifies the original proposal that the specimen is referable to *Ornithosuchus woodwardi* (Walker 1964). In the following, we discuss how the BGS GSM Elgin A skeleton differs from *Ornithosuchus* and other known ornithosuchids, and discuss the phylogenetic distribution of key characteristics (from our phylogenetic dataset) of BGS GSM Elgin A within Archosauriformes, with a particular emphasis on those widespread in Archosauria and Pseudosuchia:

- Horizontally oriented premaxilla (Ch. 29–0) bearing four premaxillary teeth (Ch. 42–2) that occupy the entire length of the premaxilla (Ch. 26–0) (Fig. 15C–E). This condition differs from *O. woodwardi* and other ornithosuchids, which have a downturned premaxilla, with three teeth that are separated from the maxilla by a large subnarial gap and a diastema equal to two tooth positions in length (Ch. 13–1 in Nesbitt 2011) (Fig. 15A). This combination of character states also allows us to distinguish BGS GSM Elgin A from the following clades: (a) Phytosauria, which have a higher tooth count, extremely elongated premaxillary body and external nares that are oriented dorsally and retracted along the snout

https://doi.org/10.1017/S1755691020000109 Published online by Cambridge University Press

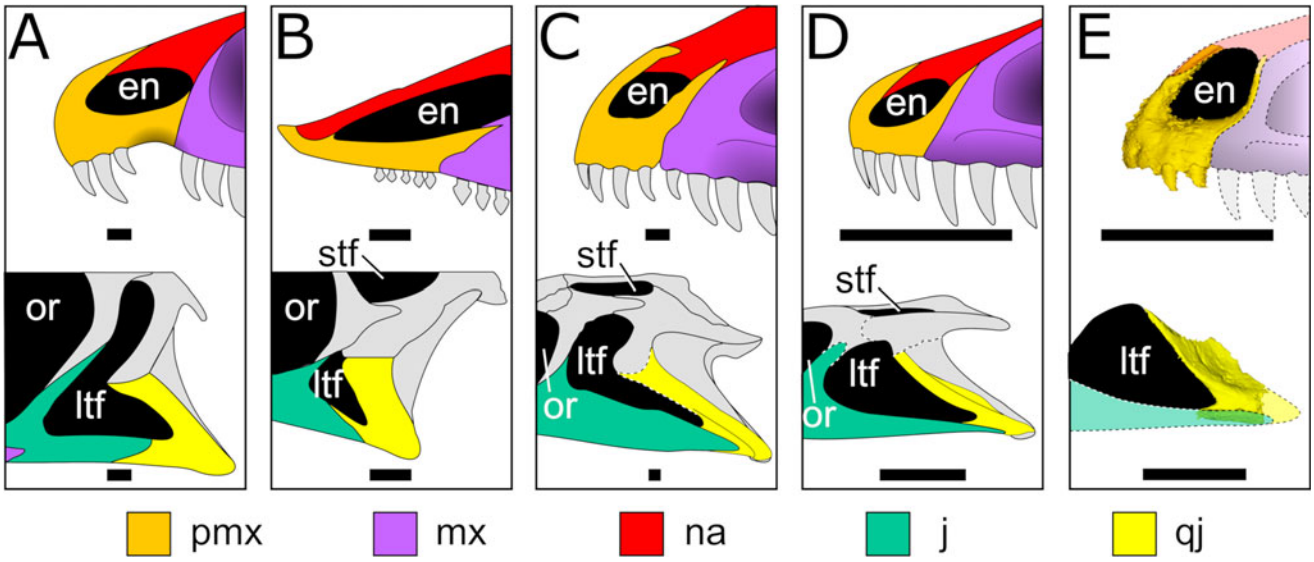

Figure 15 Comparisons of the anterior snout (top row) and jugal–quadratojugal of selected pseudosuchians. (A) *Ornithosuchus woodwardi* (modified from Walker 1964); (B) *Stagonolepis robertsoni* (redrawn and modified from Desojo *et al*. 2013); (C) *Tarjadia ruthae* (redrawn and modified from Ezcurra *et al*. 2017); (D) *Erpetosuchus granti* (redrawn and modified from Benton & Walker 2002); (E) Erpetosuchidae indet., BGS GSM Elgin A. Note the small size of the premaxilla relative to the quadrate in the depicted erpetosuchids. Abbreviations: en = external naris; j = jugal; ltf = lower temporal fenestra; mx = maxilla; na = nasal; or = orbit; pmx = premaxilla; qj = quadratojugal; stf = supratemporal fenestra. Scale bars = 10 mm.

(Stocker & Butler 2013; Stocker *et al*. 2017; Jones & Butler 2018); (b) Aetosauria, which have an edentulous anterior premaxilla, long premaxillary body (Fig. 15B) and higher tooth count (except, perhaps, for *Stagonolepis* and *Aetosaurus ferratus*) (Desojo *et al*. 2013; Parker 2018); (c) Crocodylomorpha, which have a subnarial gap to receive an enlarged dentary tooth (Nesbitt 2011); and (d) Gracilisuchidae (Butler *et al*. 2014), which have three premaxillary teeth (e.g., *Gracilisucus* – MCZ 4117). However, the combination of premaxillary features seen in BGS GSM Elgin A is not unique among pseudosuchians and can be also found in erpetosuchids (Fig. 16C–E) and some 'rauisuchians' (e.g., *Postosuchus kirkpatricki*; *Batrachotomus kupferzellensis* – SMNS 80260; Nesbitt 2011; Weinbaum 2011; Nesbitt *et al*. 2013; Tolchard *et al*. 2019).

- The jugal posterior process lies ventral to the quadratojugal (Ch. 105–1) and reaches past the posterior end of the infratemporal fenestra (Ch. 106–1) (Fig. 15C–E). In the ornithosuchids *Ornithosuchus* and *Riojasuchus*, the jugal posterior process lies dorsal to the quadratojugal and does not reach the posterior margin of the infratemporal fenestra (Fig. 15A). Within Archosauriformes, the character states present in BGS GSM Elgin A are shared with Erpetosuchidae (Figs 5, 15C–E), Crocodylomorpha, Phytosauria (except *Diandongosuchus fuyuanensis*) (Nesbitt 2011; Stocker *et al*. 2017) and, among 'rauisuchians', with *B. kupferzellensis* (SMNS 80260) and *P. kirkpatricki* (TTU-P 9000) (Gower 1999; Nesbitt 2011; Weinbaum 2011; Nesbitt *et al*. 2013).
- The dorsal process (= ascending process) of the quadratojugal is strongly anteriorly inclined at an acute angle (equal to or less than ~40–45°) from the horizontal plane (Ch. 636–1) (Fig. 15). BGS GSM Elgin A shares this character state with some members of Ornithosuchidae (e.g., *O. woodwardi* and *Riojasuchus tenuisceps*, but not *Venaticosuchus rusconi*; Walker 1964; Von Baczko & Ezcurra 2013, 2016; Von Bazcko et al. 2014, 2018). However, it is worth noting that this feature is a putative synapomorphy shared between Ornithosuchidae and Erpetosuchidae, and is one of the character states that has united these lineages into a clade in recent analyses (see

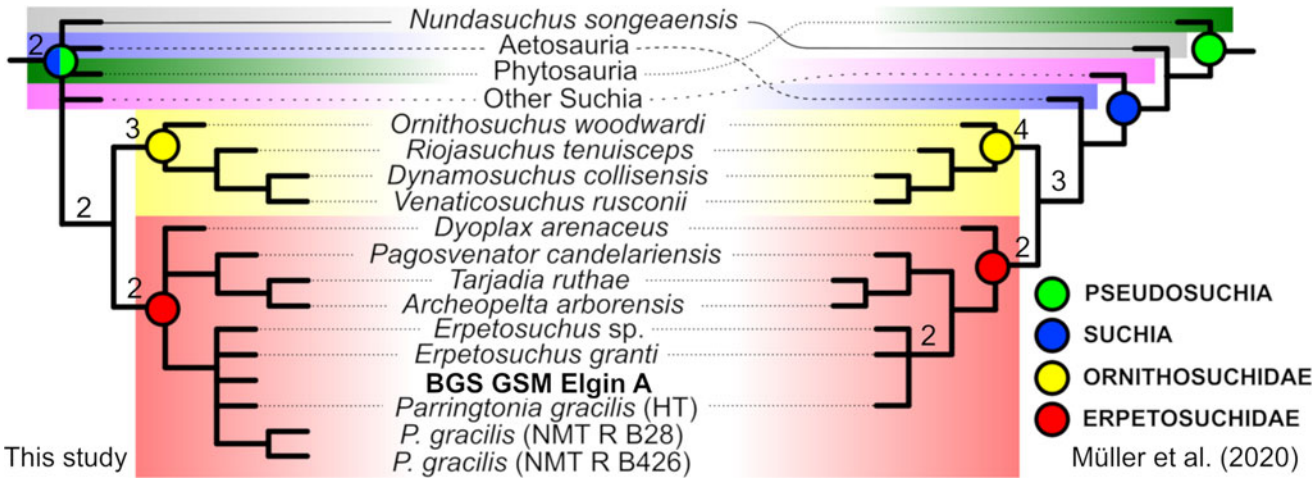

Figure 16 Phylogenetic tree of Pseudosuchia. Comparisons of the strict consensus obtained in this study (left) and Müller *et al*. (2020). Note the change of the position of Phytosauria and *Nundasuchus songaensis* and the loss of definition at the base of Pseudosuchia in this study. Numbers indicate Bremer support values above one.

https://doi.org/10.1017/S1755691020000109 Published online by Cambridge University Press

Von Baczko & Desojo 2016; Ezcurra *et al*. 2017; Lacerda *et al*. 2018) (Fig. 15A, C–E). The majority of other archosauriform groups (including 'rauisuchians' and Crocodylomorpha) either have a vertical or only marginally anteriorly inclined process, except aetosaurs (e.g., *Stagonolepis robertsoni*), in which the anterior process of the quadratojugal is posteriorly inclined (Desojo *et al*. 2013) (Fig. 15B).

- Extended surangular shelf (Ch. 286–3). Although small, the only surangular fragment found in BGS GSM Elgin A demonstrates that it had a strongly laterally extended surangular shelf (Fig. 9). This character state is present in both Ornithosuchidae and Erpetosuchidae (Ezcurra 2016; Von Baczko & Ezcurra 2016; Ezcurra *et al*. 2017), but also Erythrosuchidae (Butler *et al*. 2019a) and Proterochampsidae (Dilkes & Arcucci 2012).
- Osteoderms are densely ornamented (Ch. 589–1), have a longitudinal keel (on paramedian osteoderms, Ch. 591–1) and are longitudinally curved (Ch. 598–1) (Fig. 11E, L–O). The osteoderms of BGS GSM Elgin A share these features with other erpetosuchids (Benton & Walker 2002; Nesbitt & Butler 2013; Ezcurra *et al*. 2017). By contrast, the osteoderms of *O. woodwardi* have a longitudinal keel, are weakly sculptured and flat (Walker 1964; Von Baczko & Ezcurra 2016).
- Fibula: position of the attachment of the M. iliofibularis (Ch. 530–0) (Fig. 13O). The low platform for the attachment of the M. iliofibularis is located near the proximal end of the fibula in BGS GSM Elgin A, the erpetosuchid *Parringtonia gracilis* (NMT RB28), *Gracilisuchus* and *Mandasuchus*, whereas it is located at midshaft or closer to midshaft in phytosaurs, ornithosuchids and most 'rauisuchians' (Nesbitt 2011; Butler *et al*. 2018).

The combination of features present in BGS GSM Elgin A is inconsistent with its original identification as *Ornithosuchus* (Walker 1964), but also unambiguously distinguish it from other ornithosuchids, phytosaurs, aetosaurs 'rauisuchians' and crocodylomorphs. However, even though BGS GSM Elgin A is missing some of the bones that possess the most typical synapomorphies of Erpetosuchidae (e.g., maxilla: alveolar margin of the maxilla restricted to the anterior half of the bone), it possesses a combination of features in the cranial (premaxilla, frontal, quadrate/quadratojugal) and postcranial skeleton (hind limbs and osteoderms) that are unique to Erpetosuchidae. These are: four premaxillary teeth, evenly distributed along the alveolar margin (absence of subnarial gap); strongly ornamented frontal; posterior process of the jugal that reaches close to the quadrate condyles (posterior to the lower temporal fenestra caudal margin), and articulates ventral to the quadratojugal anterior process; strongly anteriorly inclined quadrate axis/quadratojugal anterior process (<45°); and four rows of strongly ornamented osteoderms per vertebral segment (two per side).

There are, however, also significant differences between BGS GSM Elgin A and other known erpetosuchids, including the sympatric *Erpetosuchus granti*. These include:

- The presence of a foramen on the lateral surface of the premaxilla between P1 and P2, the markedly triangular external nares and the 'step-shaped' posterodorsal process of the premaxilla) (all represent potential autapomorphies within Erpetosuchidae) (Fig. 6). These features of BGS GSM Elgin A are previously unreported in *E. granti* (although this may be also due to the lack of details in the holotype moulds) or any other erpetosuchid (Fig. 15D). However, a foramen above P1/P2 is present in specimens of *Parringtonia* and it is unclear whether *Tarjadia* also has one. Additionally, in BGS GSM Elgin A the palatal process of the premaxilla is concave posteriorly (Fig. 6F), as opposed to straight in *E. granti* (NHMUK PV R3139; Benton & Walker 2002).
- Unfused frontals and contact with the parietal (Ch.112–0 and Ch.116–2) (Fig. 6H–S). Similar to *Tarjadia ruthae* and *Parringtonia gracilis*, the frontals of BGS GSM Elgin A are unfused along the midline (see Ezcurra *et al*. 2017). Benton & Walker (2002) reported that the frontals are fused in *E. granti*, but we could not confidently confirm this in our examination of the specimen. The frontals also have a complex interdigitating contact with the parietal (rather than the simple or weakly concave contact seen in all other erpetosuchids) (Benton & Walker 2002; Ezcurra *et al*. 2017; Nesbitt *et al*. 2018). Furthermore, their shape differs from *E. granti* in that they are relatively short and have a simple anterior contact with the nasal. Finally, the posterolateral corner of the frontal in BGS GSM Elgin A has an articular surface for the postfrontal (or postorbital) (Fig. 6H–J). This condition is seen in all erpetosuchids, except *E. granti* (NHMUK PV R3139), in which the postfrontal is considered to be absent (fused with the frontal; Benton & Walker 2002). However, it is noteworthy that fine details such as the sutures are hard to see in any of the moulds of any Elgin specimen.
- Frontals in ventral view (Ch. 121–1) (Fig. 6L, Q). The crista cranii that separate the orbits from the olfactory bulbs and cerebrum structures are well-developed, and tall ridges delimit the constricted the olfactory tract canal. This feature differs from the low crests seen in *P. gracilis* (Nesbitt *et al*. 2018). However, these are the only two erpetosuchids where this condition can be assessed confidently.
- Foramen on the posterior surface of the quadratojugal (potential autapomorphy) (Fig. 8). BGS GSM Elgin A has a foramen on the posterior body of the quadratojugal, which is not present in any other erpetosuchid with a preserved quadratojugal (see *Erpetosuchus* sp. in Fig. 5). This feature is, to our knowledge, unreported in any other pseudosuchian.
- Ectopterygoid (Figs 5E, F, 9A–F). The ectopterygoid of BGS GSM Elgin A is unlike those of most archosauriforms in lacking a strong curvature. Within erpetosuchids, the ectopterygoid is well preserved and strongly curved in *Erpetosuchus* sp. (AMNH 29300) (Fig. 5).
- Lack of spine table (potential autapomorphy within Erpetosuchidae) (Fig. 11). All of the available vertebrae of BGS GSM Elgin A (middle and distal caudals) lack the characteristic concave spine tables that are present in other erpetosuchids (e.g., *E. granti*, *P. gracilis*, *T. ruthae*) (Figs 2, 3) (see Benton & Walker 2002; Nesbitt & Butler 2013; Ezcurra *et al*. 2017). Note that this character is normally assessed on the cervical and dorsal vertebrae, whereas the only available vertebrae in BGS GSM Elgin A are caudals. Furthermore, caution is warranted because NMS G.1992.37.1 shows that *E. granti* has spine tables only on the cervical and anterior dorsal series (Figs 2, 3). This contrasts with *P. gracilis* and *T. ruthae*, which have a well-developed spine table on the available anterior caudal vertebrae (see Nesbitt & Butler 2013; Ezcurra *et al*. 2017), suggesting that this feature extends posterior to the dorsal vertebrae. Thus, it is possible that the lack of spine tables in dorsal (middle and posterior) and caudal vertebrae characterises BGS GSM Elgin A and *E. granti*, although this needs to be confirmed in more complete specimens.
- Shape and thickness of the osteoderms (Ch. 595–1 and Ch. 592–1) (potential autapomorphy within Erpetosuchidae) (Fig. 11L–O). The paramedian osteoderms of BGS GSM Elgin A are slightly longer than wide, as in *P. gracilis* (NHMUK PV R8646) and *E. granti* (NHMUK PV R3139), unlike the condition in *T. ruthae*, *Archeopelta arborensis*, *Pagosvenator candelariensis* and other specimens referred to *P. gracilis* (NMT RB426, NMT RB28), which either have

https://doi.org/10.1017/S1755691020000109 Published online by Cambridge University Press

square or wider-than-long osteoderms (Benton & Walker 2002; Nesbitt & Butler 2013; Ezcurra *et al*. 2017; Lacerda *et al*. 2018). The osteoderms of BGS GSM Elgin A are notably thin (Fig. 11N–O), contrasting with the thicker osteoderms of other erpetosuchids (although this may be due to the smaller body size of BGS GSM Elgin A compared to most other erpetosuchids except *Erpetosuchus* and *Dyoplax arenaceous*) (Lucas *et al*. 1998; Benton & Walker 2002; Maisch *et al*. 2013). Their positions (e.g., alignment relative to the vertebral column, imbrication) and ornamentation are similar to those of other erpetosuchids.

- Thin-walled femur (Ch. 508–1) (potential autapomorphy within Erpetosuchidae). Perhaps linked with its gracile morphology (shared with *E. granti* and, likely, *P. gracilis*, but not *T. ruthae*), the femora of BGS GSM Elgin A is uniquely thin-walled (thickness/diameter ratio <0.3 at the midshaft). This is thinner than in the femora of *P. gracilis* (NMT RB28, NMT RB426) and *T. ruthae*.

3.2. Results of the phylogenetic analyses

Our phylogenetic analysis found 110 MPTs with lengths of 3410 steps, consistency index = 0.256 and retention index = 0.636. BGS GSM Elgin A is recovered within Erpetosuchidae, closely related to *Erpetosuchus* and *Parringtonia* (Fig. 16; supplementary Fig. S2). Overall, Erpetosuchidae is supported by one unambiguous (present in all MPTs) and 22 ambiguous (not shared in all MPTs) synapomorphies, five of which can be scored in BGS GSM Elgin A: (1) prominent ornamentation of the dorsal surface of the skull (frontal) (Ch. 5: 1→2); (2) orbital margin of the frontal is slightly raised above the skull table (Ch. 7: 0→1); (3) multiple rows of dorsal osteoderms (Ch. 588: 2→3) – reversed to state 2 in BGS GSM Elgin A; (4) strongly ornamented osteoderms (Ch. 589: 0→1); (5) thick paramedian osteoderms (Ch. 592: 0→1) – reversed to state 0 in *Parringtonia*, *Erpetosuchus* and BGS GSM Elgin A. The relationships within Erpetosuchidae are largely consistent, although weaker (see Bremer values in Fig. 16 and supplementary Fig. S2) with those recovered in previous iterations of the phylogenetic dataset: erpetosuchids are divided into two clades (Pagosvenator candelariensis (Tarjadia ruthae + Archeopelta arborensis)) and (*Erpetosuchus* + *Parringtonia*) (Müller *et al*. 2020). However, these groups are in a polytomy with *Dyoplax arenaceous*, differing from the results of Ezcurra *et al*. (2017) and Müller *et al*. (2020), both of which found *D. arenaceous* to be the earliest diverging erpetosuchid. BGS GSM Elgin A is in a polytomy with specimens of *Erpetosuchus* spp. and *Parringtonia gracilis* (holotype: NHMUK PV R8646, NMT RB28, NMT RB426) (Fig. 16; supplementary Fig. S2).

As in other recent studies, Erpetosuchidae is recovered as the sister taxon to Ornithosuchidae (Von Baczko & Desojo 2016; Ezcurra *et al*. 2017; Lacerda *et al*. 2018; Müller *et al*. 2020) in a clade supported by six unambiguous and nine ambiguous synapomorphies. However, unlike these other studies, the relationships of this clade with others in Pseudosuchia are unclear. Specifically, whereas we recovered other historically well-established clades such as Phytosauria, Aetosauria, Gracilisuchidae, Poposauroidea and Rauisuchidae (the latter in a poorly defined suchian clade with paracrocodylomorphs), all of these clades are found in an unresolved polytomy with *Nundasuchus songeaensis* and Ornithosuchidae + Erpetosuchidae. Note that the support for these clades remains moderate to high (Bremer support ranging from 2 to 5) when they are considered individually (supplementary Fig. S2), meaning that the changes in our datasets affected only their relative positions within Pseudosuchia. The monophyly of Pseudosuchia is supported by six unambiguous and 14 ambiguous synapomorphies (see Supplementary material) and the clade has a Bremer support of 2.

The poor resolution in this area of the tree is not entirely surprising given the historical low support for relationships at the base of Pseudosuchia (Fig. 16; supplementary Fig. S2) (Nesbitt 2011; Irmis *et al*. 2013; Ezcurra 2016; Ezcurra *et al*. 2017; Müller *et al*. 2020). The addition of the new terminal taxa may have weakened support by introducing a series of issues into the analyses including: polarity, which is aggravated by the limited taxonomic sampling of some lineages (e.g., Suchia, Paracrocodylomorpha, Crocodylomorpha); character conflicts introduced with the updated scores of old and new operational taxonomic units (particularly in postcranial characters); and high homoplasy amongst pseudosuchian lineages. We suggest that the inclusion of more complete paracrocodylomorph and crocodylomorph terminal taxa and the addition of novel characters – as outlined for Crocodylomorpha by Irmis *et al*. (2013) – would help to resolve the relationships of well-established groups within Pseudosuchia.

3.3. Erpetosuchidae indet., *Erpetosuchus granti* or a new species?

As shown above, BGS GSM Elgin A shares synapomorphies with Erpetosuchidae and *E. granti*, but also differs from other erpetosuchids and therefore could potentially represent a new species. Specifically, BGS GSM Elgin A differs from other erpetosuchids in having: a large foramen on the lateral side of the premaxilla between P1/P2 (also present in *Parringtonia gracilis* and potentially in *Tarjadia ruthae*; other erpetosuchids are too poorly preserved to verify this character); a 'step-shaped' posterior edge of the premaxilla in lateral view, with the posterior margin of the premaxilla anterior to the posteroventral corner of the external nares; external nares that are triangular in shape; a straight body of the ectopterygoid; a foramen on the occipital surface of the quadratojugal; an unusually thin femoral wall (transverse thickness of bone wall/femoral diameter <0.3); thin osteoderms (shared with *E. granti* and *P. gracilis*); and neural spines of the caudal vertebrae that lack spine tables (potentially shared with *E. granti*). BGS GSM Elgin A is considerably smaller than *Tarjadia*, *Parringtonia* and *Pagosvenator*, and is comparable in size only with *Dyoplax* and other *Erpetosuchus* specimens (Fig. 17). Nevertheless, we refrain from assigning BGS GSM Elgin A to *E. granti* or erecting a new taxon because the limited overlap between BGS GSM Elgin A and the specimens referred to *Erpetosuchus* prevents us from fully comparing these specimens.

Unfortunately, most of putative autapomorphies of BGS GSM Elgin A are lost or impossible to assess in coeval specimens of *E. granti* (Fig. 17A–D). Indeed, BGS GSM Elgin A and all known specimens of *E. granti* have very few elements in common (predominantly cranial), and even these are difficult to compare due to differential preservation. Whereas BGS GSM Elgin A comprises disarticulated cranial bones, a posterior vertebral column and hind limb material, only portions of the anterior skeletons of *E. granti* (NHMUK PV R3139 and NMS G.1992.37.1) are known (e.g., complete articulated skull, forelimbs, cervical and anterior-to-middle dorsal vertebrae, and associated osteoderms) – note also that the dorsal vertebrae of NMS G.1966.43.4 are damaged so that their neural spines are not preserved. To complicate the matter, the only known cranial material of *E. granti* is preserved in the type specimen (NHMUK PV R3139) as the mould of an articulated skull, along with the cervical series, pectoral girdle and hindlimbs. Thus, the only way to study this specimen is through casts (see Benton & Walker 2002), in which the surface details (including sutures and ornamentation) are often lost or difficult to interpret (even in first-generation casts).

On the basis of our proposed diagnosis of *E. granti*, BGS GSM Elgin A differs from *E. granti* in both of the character states for

https://doi.org/10.1017/S1755691020000109 Published online by Cambridge University Press

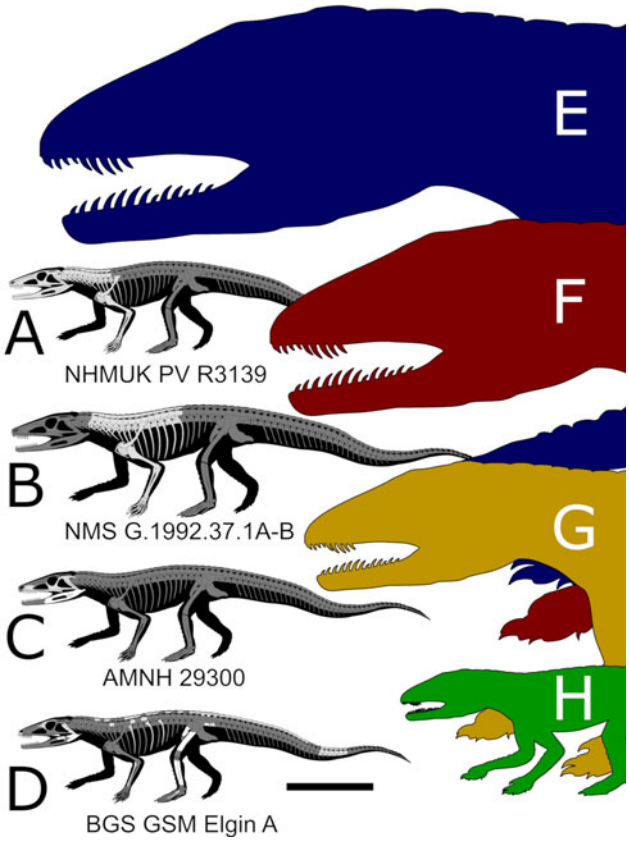

Figure 17 Skeletal reconstructions showing preserved bones in BGS GSM Elgin A and specimens referred to *Erpetosuchus*, and size comparisons with other erpetosuchids. (A) *Erpetosuchus granti*, NHMUK PV R3139; (B) *E. granti*, NMS G.1992.37.1; (C) *Erpetosuchus* sp. AMNH 29300; (D) Erpetosuchidae indet, BGS GSM Elgin A; (E) *Tarjadia ruthae*; (F) *Pagosvenator candelariensis*; (G) *Parringtonia gracilis*; (H) *Dyoplax arenaceous.* Silhouettes in (E–G), modified from Ezcurra *et al.* (2017). Scale bar = 5 cm.

which the specimens can be assessed. Specifically: (1) the angle between the alveolar margin and the anterior margin of the premaxilla in lateral view is acute in BGS GSM Elgin A and obtuse in *E. granti*; and (2) the paramedian osteoderms of *E. granti* have an unornamented anterior lamina that is absent in the osteoderms of BGS GSM Elgin A. However, as previously reported, the neural arches of the caudal vertebrae of BGS GSM Elgin A lack spine tables – a feature that might unite it with *E. granti*, but that cannot be confirmed in the absence of more complete specimens.

The CT scans of *Erpetosuchus* sp. (AMNH 29300) are also of limited use. The elements common to both BGS GSM Elgin A and AMNH 29300 (quadratojugal, ectopterygoid, surangular shelf) are very similar and, if informative, they are not diagnostic below the family level (Figs 5, 8, 10, 11, 15). The only differences we notice are that the curvature of the ectopterygoid in BGS GSM Elgin A is less pronounced than that of AMNH 29300, and the foramen on the quadratojugal of BGS GSM Elgin A is absent in AMNH 29300 (compare Figs 5G–H, 8).

Overall, the series of features that distinguish BGS GSM Elgin A from other taxa (e.g., P1/P2 foramen; the shape of the posterodorsal process of the premaxilla; the shape of the external nares; unfused frontals; suture and ornamentation of the frontal; the curvature of the ectopterygoid) are unfortunately missing or inaccessible in other specimens referred to *Erpetosuchus.* Thus, we find the previously discussed verifiable differences and similarities insufficient to conclusively prove that BGS GSM Elgin A distinct from *Erpetosuchus granti*. Nevertheless, it is useful to summarise the two possible options:

(a) BGS GSM Elgin A is a new species. In this case, the differences noted between BGS GSM Elgin A and *Erpetosuchus* specimens are not simply expressions of intraspecific variation. This might hint at a higher diversity for the Lossiemouth Sandstone reptile assemblage than previously realised. Moreover, it would represent the first example of two sympatric erpetosuchids, perhaps indicating niche partitioning.

(b) Alternatively, BGS GSM Elgin A is referable to *E. granti*. In this case, the unique features of BGS GSM Elgin A would represent individual variation within *E. granti* or perhaps the expression of an earlier ontogenetic stage or features of the taxon that are not visible in other specimens lacking these elements. One line of evidence that points towards BGS GSM Elgin A being sub-adult comes from the impressions left by the brain on the frontal (Fig. 6I). In living crocodylian species, there is a close relationship between the brain and skull roof in early ontogeny, with lengthening and separation of the olfactory lobes from the rest of the cerebrum during early adulthood (Jirak & Janacek 2017). Adult crocodylian brain cavity endocasts largely represent the dural cavity (Witmer *et al.* 2008), and lack the impression of the bony ridge that records the position of the interhemispheric fissure. Since BGS GSM Elgin A exhibits clear separation of the telencephalic fossa and an elongate olfactory tract, it seems likely that the individual was neither a young juvenile nor fully adult. However, since adult retention of a paedomorphic condition is also possible, this evidence remains inconclusive. If this were confirmed by any further discoveries in the future, the putative autapomorphies of BGS GSM Elgin A could help to refine the diagnosis of *Erpetosuchus.*

These questions can only be answered with the discovery of better-preserved specimens with elements shared in common with the currently known specimens of *Erpetosuchus* and BGS GSM Elgin A.

4. Conclusions

We present a revision of some of the erpetosuchid material from the LSF using μCT scans. This work includes the first description of the fossil content of BGS GSM 91072–81, 91085–6. We show that numerous bones belonging to at least two different species are hidden therein. The original identification of one of these skeletons (BGS GSM Elgin A) as *Ornithosuchus* is rejected, and we show, instead, that it is a gracile, small-bodied (perhaps juvenile) erpetosuchid. Detailed osteological comparisons between BGS GSM Elgin A and the coeval *Erpetosuchus granti* reveal strong similarities, but also some crucial differences. In addition, we provide new descriptive information for *E. granti* based on new μCT scans of a referred specimen. This work revealed previously unknown characteristics of the forelimb and allowed us to propose an updated diagnosis for *E. granti*. Our phylogenetic analysis suggests that BGS GSM Elgin A is closely related to *Erpetosuchus* but does not clarify whether or not it represents a new taxon, an issue exacerbated by the lack of anatomical overlap between key specimens. Under these circumstances, the evidence is insufficient to choose between the competing hypotheses that BGS GSM Elgin A is either a small or juvenile *E. granti*, or a new taxon. Nevertheless, we identified a number of potentially diagnostic features for BGS GSM Elgin A in the hope that they could be used as a guide to clarify the

https://doi.org/10.1017/S1755691020000109 Published online by Cambridge University Press

relationships of BGS GSM Elgin A and *Erpetosuchus* in the light of future discoveries.

The second specimen (BGS GSM Elgin P) included in these blocks is a new specimen of the procolophonid parareptile *Leptopleuron lacertinum*. The significance of the fossil content of the BGS GSM 91072–81, 91085–6, therefore, goes beyond their taxonomic and systematic importance. By identifying these 'new' specimens in historical material, our study suggests that the richness of the 'Elgin reptile fauna' might have been seriously underestimated. It is possible that – concealed within collections and the few active exposures – similar remains are more common than previously thought.

Finally, our study demonstrates that μCT scanning techniques are an invaluable tool for extracting new and heretofore inaccessible data from small-to-medium-sized Elgin specimens regardless of their preservation and preparation history.

5. Data availability

All 3D models and μCT datasets used in this studied were uploaded to Morphosource (https://www.morphosource.org/) and can be freely accessed at [https://www.morphosource.org/MyProjects/Dashboard/dashboard/select_project_id/1115] (Davis *et al*. 2017).

6. Supplementary material

Supplementary material is available online at https://doi.org/10.1017/S1755691020000109

7. Acknowledgements

This work would have not been possible without access to the specimens in the BGS, NMS and NHMUK. For this reason, we particularly thank Mr Paul Shepherd (BGS), Dr Susannah Maidment (NHMUK) and the NMS staff for facilitating DF's visits to these collections. We are grateful to Dr Alice Macente, Dr Tom G. Davies and Dr Elizabeth Martin-Silverstone for guidance and assistance during the CT scanning of the NMS and BGS specimens, and to Dr Mark A. Norell for permission and Dr Morgan Hill for scanning AMNH 29300. DF is grateful to Dr Alessandro Chiarenza for useful discussions and assistance with TNT software. Field photos used in Figure 1 were kindly provided by Mr David Longstaff (Elgin Museum) and NCF. This research is part of a larger project founded by the Royal Commission for the Exhibition of 1851 – Science Fellowship awarded to DF. We would like to thank the two reviewers and editor whose insightful comments greatly improved the quality of this manuscript.

8. References

Bennett, S. C. 2020. Reassessment of the Triassic archosauriform *Scleromochlus taylori*: neither runner nor biped, but hopper. *PeerJ* **8**, e8418.

Benton, M. J. & Walker, A. D. 1985. Palaeoecology, taphonomy, and dating of Permo-Triassic reptiles from Elgin, north-east Scotland. *Palaeontology* **28**, 207–34.

Benton, M. J. & Walker, A. D. 2002. *Erpetosuchus*, a crocodile-like basal archosaur from the Late Triassic of Elgin, Scotland. *Zoological Journal of the Linnean Society* **136**, 25–47.

Benton, M. J. & Walker, A. D. 2011. *Saltopus*, a dinosauriform from the Upper Triassic of Scotland. *Earth and Environmental Science Transactions of the Royal Society of Edinburgh* **101**, 285–99.

Butler, R. J., Sullivan, C., Ezcurra, M. D., Liu, J., Lecuona, A. & Sookias, R. B. 2014. New clade of enigmatic early archosaurs yields insights into early pseudosuchian phylogeny and the biogeography of the archosaur radiation. *BMC Evolutionary Biology* **14**, 128.

Butler, R. J., Nesbitt, S. J., Charig, A. J., Gower, D. J. & Barrett, P. M. 2018. *Mandasuchus tanyauchen*, gen. et sp. nov., a pseudosuchian archosaur from the Manda Beds (?Middle Triassic) of Tanzania. *In* Sidor, C. A. & Nesbitt, S. J. (eds) *Vertebrate and climatic evolution in the Triassic rift basins of Tanzania and Zambia*, **17**, 96–121. Society of Vertebrate Paleontology Memoir.

Butler, R. J., Sennikov, A. G., Dunne, E. M., Ezcurra, M. D., Hedrick, B. P., Maidment, S. C. R., Meade, L. E., Raven, T. J. & Gower, D. J. 2019a. Cranial anatomy and taxonomy of the erythrosuchid archosauriform '*Vjushkovia triplicostata*' Huene, 1960, from the Early Triassic of European Russia. *Royal Society Open Science* **6**, 191289.

Butler, R. J., Sennikov, A. G., Ezcurra, M. D. & Gower, D. J. 2019b. The last erythrosuchid? A revision of *Chalishevia cothurnata* Ochev, 1980 from the late Middle Triassic of European Russia. *Acta Palaeontologica Polonica* **64**, 757–74.

Cabreira, S. F., Kellner, A., Dias-da-Silva, S., Roberto da Silva, L., Bronzati, M., Marsola, J., Müller, R. T., Bittencourt, J. S., Batista, B. J., Raugust, T., Carrilho, R., Brodt, A. & & Langer, M. C. 2016. A unique Late Triassic dinosauromorph assemblage reveals dinosaur ancestral anatomy and diet. *Current Biology* **26**, 3090–95.

Chatterjee, S. 1985. *Postosuchus*, a new thecodontian reptile from the Triassic of Texas and the origin of tyrannosaurs. *Philosophical Transactions of the Royal Society of London. Series B, Biological Sciences* **309**, 395–460.

Clark, J. M., Sues, H.-D. & Berman, D. S. 2000. A new specimen of *Hesperosuchus agilis* from the Upper Triassic of New Mexico and the interrelationships of basal crocodylomorph archosaurs. *Journal of Vertebrate Paleontology* **20**, 683–704.

Cope, E. D. 1869. Synopsis of the extinct Batrachia, Reptilia, and Aves of North America. *Transactions of the American Philosophical Society* **14**, 1–252.

Cunningham, J. A., Rahman, I. A., Lautenschlager, S., Rayfield, E. J. & Donoghue, P. C. J. 2014. A virtual world of paleontology. *Trends in Ecology and Evolution* **29**, 347–57.

Davies, T. G., Rahman, I. A., Lautenschlager, S., Cunningham, J. A., Asher, R. J., Barrett, P. M., Bates, K. T., Bengtson, S., Benson, R. B. J., Boyer, D. M., Braga, J., Bright, J. A., Claessens, L. P. A. M., Cox, P. G., Dong, X.-P., Evans, A. R., Falkingham, P. L., Friedman, M., Garwood, R. J., Goswami, A., Hutchinson, J. R., Jeffery, N. S., Johanson, Z., Lebrun, R., Martínez-Pérez, C., Marugán-Lobón, J., O'Higgins, P. M., Metscher, B., Orliac, M., Rowe, T. B., Rücklin, M., Sánchez-Villagra, M. R., Shubin, N. H., Smith, S. Y., Starck, J. M., Stringer, C., Summers, A. P., Sutton, M. D., Walsh, S. A., Weisbecker, V., Witmer, L. M., Wroe, S., Yin, Z., Rayfield, E. J. & Donoghue, P. C. J. 2017. Open data and digital morphology. *Proceedings of the Royal Society B* **284**, 20170194.

Desojo, J. B., Heckert, A. B., Martz, J. W., Parker, W. G., Schoch, R. R., Small, B. J. & Sulej, T. 2013. Aetosauria: a clade of armoured pseudosuchians from the Upper Triassic continental beds. *In* Nesbitt, S. J., Desojo, J. B. & Irmis, R. B. (eds) *Anatomy, phylogeny and palaeobiology of early archosaurs and their kin*, **379**, 203–39. Geological Society of London, Special Publication.

Dilkes, D. W. & Arcucci, A. B. 2012. *Proterochampsa barrionuevoi* (Archosauriformes: Proterochampsia) from the Late Triassic (Carnian) of Argentina and a phylogenetic analysis of Proterochampsia. *Palaeontology* **55**, 853–85.

Ezcurra, M. D. 2016. The phylogenetic relationships of basal archosauromorphs, with an emphasis on the systematics of proterosuchian archosauriforms. *PeerJ* **4**, e1778.

Ezcurra, M. D., Fiorelli, L. E., Martinelli, A. G., Rocher, S. M., Von Baczko, B., Ezpeleta, M., Taborda, J. R. A., Hechenleitner, E. M., Trotteyn, M. J. & Desojo, J. B. 2017. Deep faunistic changes preceded the raise of dinosaurs in southwestern Pangaea. *Nature Ecology & Evolution* **1**, 1477–83.

Frostick, L., Reid, I., Jarvis, J. & Eardley, H. 1988. Triassic sediments of the Inner Moray Firth, Scotland: early rift deposits. *Journal of the Geological Society* **145**, 235–48.

Gauthier, J. & Padian, K. 1985. Phylogenetic, functional, and aerodynamic analyses of the origin of birds and their flight. *In* Hecht, M. K., Ostrom, J. H., Viohl, G. & Wellnhofer, P. (eds) *The beginning of birds*, 185–97. Eichstatt: Freunde des Jura-Museums.

Goloboff, P. A., Farris, J. S. & Nixon, K. C. 2008. TNT: a free program for phylogenetic analysis. *Cladistics* **24**, 774–86.

Gordon, G. 1859. On the geology of the lower and western part of the province of Moray: its history, present state of enquiry and points for future examination. *Edinburgh New Philosophical Journal, New Series* **9**, 14–58.

Gower, D. J. 1999. Cranial osteology of a new rauisuchian archosaur from the Middle Triassic of southern Germany. *Stuttgarter Beiträge zur Naturkunde B* **280**, 1–49.

Gower, D. J. 2003. Osteology of the early archosaurian reptile *Erythrosuchus africanus* Broom. *Annals of the South African Museum* **110**, 1–84.

Irmis, R. B., Nesbitt, S. J. & Sues H.-D. 2013. Early Crocodylomorpha. *In* Nesbitt S. J., Desojo J. B. & Irmis R. B. (eds) *Anatomy, phylogeny and palaeobiology of early archosaurs and their kin*, **379**, 275–302. Geological Society, London, Special Publications.

Jirak, D. & Janacek, J. 2017 Volume of the crocodilian brain and endocast during ontogeny. *PLoS ONE* **12**, e0178491.

Jones, A. S. & Butler, R. J. 2018. A new phylogenetic analysis of Phytosauria (Archosauria: Pseudosuchia) with the application of continuous and geometric morphometric character coding. *PeerJ* **6**, e5901.

Keeble, E. & Benton, M. J. 2020. Three-dimensional tomographic study of dermal armour from the tail of the Triassic aetosaur *Stagonolepis robertsoni*. *Scottish Journal of Geology* **56**, 55–62. doi: 10.1144/sjg2019-026.

Krebs, B. 1974. Die Archosaurier. *Naturwissenschaften* **61**, 17–24.

Lacerda, M. B., de Franca, M. A. G. & Schultz, C. L. 2018. A new erpetosuchid (Pseudosuchia, Archosauria) from the Middle–Late Triassic of southern Brazil. *Zoological Journal of the Linnean Society* **184**, 804–24.

Langer, M. C. & Benton, M. J. 2006. Early dinosaurs: a phylogenetic study. *Journal of Systematic Palaeontology* **4**, 309–58.

Lessner, E. J., Stocker, M. R., Smith, N. D., Turner, A. H., Irmis, R. B. & Nesbitt, S. J. 2016. A new rauisuchid (Archosauria, Pseudosuchia) from the Upper Triassic (Norian) of New Mexico increases the diversity and temporal range of the clade. *PeerJ* **4**, e2336.

Lucas, S. G., Wild, R. & Hunt, A. T. 1998. *Dyoplax* O. Fraas, a Triassic sphenosuchian from Germany. *Stuttgarter Beiträge zur Naturkunde B* **263**, 1–13.

Maisch, M. W., Matzke, A. T. & Rathgeber, T. 2013. Re-evaluation of the enigmatic archosaur *Dyoplax arenaceus* O. Fraas, 1867 from the Schilfsandstein (Stuttgart Formation, lower Carnian, Upper Triassic) of Stuttgart, Germany. *Neues Jahrbuch für Geologie und Paläontologie, Abhandlungen* **267**, 353–62.

Martin, J. C. 1860. A ramble among the fossiliferous beds of Moray. 9 pp. Unpublished MS held by Elgin Museum.

Mastrantonio, B. M., Von Baczko, M. B., Desojo, J. B. & Schultz, C. L. 2019. The skull anatomy and cranial endocast of the pseudosuchid archosaur *Prestosuchus chiniquensis* from the Triassic of Brazil. *Acta Palaeontologica Polonica* **64**, 171–98.

Müller, R. T., Langer, M. C. & Dias-da-Silva, S. 2018. An exceptionally preserved association of complete dinosaur skeletons reveals the oldest long-necked sauropodomorphs. *Biology Letters* **14**, 20180633.

Müller, R. T., Von Baczko, M. B., Desojo, J. B. & Nesbitt, S. J. 2020. The first ornithosuchid from Brazil and its macroevolutionary and phylogenetic implications for Late Triassic faunas in Gondwana. *Acta Palaeontologica Polonica* **65**, 1–10.

Murchison, R. I. 1859. On the sandstones of Morayshire (Elgin, &c.) containing reptilian remains; and on their relations to the Old Red Sandstone of that country. *Quarterly Journal of the Geological Society* **15**, 419–39.

Nesbitt, S. J. 2007. The anatomy of *Effigia okeeffeae* (Archosauria, Suchia), theropod-like convergence, and the distribution of related taxa. *Bulletin of the American Museum of Natural History* **302**, 1–84.

Nesbitt, S. J. 2011. The early evolution of archosaurs: relationships and the origin of major clades. *Bulletin of the American Museum of Natural History* **352**, 1–292.

Nesbitt, S. J., Brusatte, S. J., Desojo, J. B., Liparini, A., De Franca, M. A. G., Weinbaum, J. C. & Gower, D. J. 2013. Rauisuchia. *In* Nesbitt S. J., Desojo J. B. & Irmis R. B. (eds) *Anatomy, phylogeny and palaeobiology of early archosaurs and their kin*, **379**, 241–74. Geological Society, London, Special Publications.

Nesbitt, S. J., Stocker, M. R., Parker, W. G., Wood, T. A., Sidor, C. A. & Angielczyk, K. D. 2018. The braincase and endocast of *Parringtonia gracilis*, a Middle Triassic suchian (Archosauria: Pseudosuchia). *In* Sidor, C. A. & Nesbitt, S. J. (eds) *Vertebrate and climatic evolution in the Triassic rift basins of Tanzania and Zambia*, **17**, 122–41. Society of Vertebrate Paleontology Memoir.

Nesbitt, S. J. & Butler, R. J. 2013. Redescription of the archosaur *Parringtonia gracilis* From the Middle Triassic Manda Beds of Tanzania, and the antiquity of Erpetosuchidae. *Geological Magazine* **150**, 225–38.

Newton, E. T. 1894. Reptiles from the Elgin Sandstone. Description of two new genera *Philosophical Transactions of the Royal Society of London, Series B: Biological Sciences* **185**, 573–607.

Olsen, P. E., Sues, H.-D. & Norell, M. A. 2001. First record of *Erpetosuchus* (Reptilia: Archosauria) from the Late Triassic of North America. *Journal of Vertebrate Paleontology* **20**, 633–36.

Parker, W. G. 2018. Anatomical notes and discussion of the first described aetosaur *Stagonolepis robertsoni* (Archosauria: Suchia) from the Upper Triassic of Europe, and the use of plesiomorphies in aetosaur biochronology. *PeerJ* **6**, e5455.

Parker, W. G., Irmis, R. B., Nesbitt, S. J., Martz, J. W. & Browne, L. S. 2005. The Late Triassic pseudosuchian *Revueltosaurus callenderi* and its implications for the diversity of early ornithischian dinosaurs. *Proceedings of the Royal Society B: Biological Sciences* **272**, 963–69.

Parrish, J. M. 1993. Phylogeny of the Crocodylotarsi, with reference to archosaurian and crurotarsan monophyly. *Journal of Vertebrate Paleontology* **12**, 287–308.

Peacock, J. D., Berridge, N. G., Harris, A. L. & May, F. 1968. *The Geology of the Elgin District* (Sheet 95). Memoirs of the Geological Survey of Scotland, HMSO, Edinburgh, 155 pp.

Roberto-Da-Silva, L., França, M. A. G., Cabreira, S. F., Müller, R. T. & Dias-Da-Silva, S. 2016. On the presence of the subnarial foramen in *Prestosuchus chiniquensis* (Pseudosuchia: Loricata) with remarks on its phylogenetic distribution. *Anais da Academia Brasileira de Ciências* **88**, 1309–23.

Säilä, L. 2010. Osteology of *Leptopleuron lacertinum* Owen, a procolophonoid parareptile from the Upper Triassic of Scotland, with remarks on ontogeny, ecology and affinities. *Earth and Environmental Science Transactions of the Royal Society of Edinburgh* **101**, 1–25.

Schachner, E. R., Irmis, R. B., Huttenlocker, A. K., Sanders, K., Cieri, R. L. & Nesbitt, S. J. 2020. Osteology of the Late Triassic bipedal archosaur *Poposaurus gracilis* (Archosauria: Pseudosuchia) from Western North America. *Anatomical Record* **303**, 874–917.

Sereno, P. C. 1991. Basal archosaurs: phylogenetic relationships and functional implications. *Society of Vertebrate Paleontology Memoir* **2**, 1–53.

Sereno, P. C., Forster, C. A., Rogers, R. R. & Moneta, A. M. 1993. Primitive dinosaur skeleton from Argentina and the early evolution of the Dinosauria. *Nature* **361**, 64–66.

Sereno, P. C., McAllister, S. & Brusatte, S. L. 2005. Taxonsearch: a relational database for suprageneric taxa and phylogenetic definitions. *PhyloInformatics* **8**, 1–21.

Sereno, P. C., Martínez, R. N. & Alcober, O. A. 2013. Osteology of *Eoraptor lunensis* (Dinosauria, Sauropodomorpha). Basal sauropodomorphs and the vertebrate fossil record of the Ischigualasto Formation (Late Triassic: Carnian-Norian) of Argentina. *Journal of Vertebrate Paleontology Memoir* **12**, 83–179.

Stocker, M. R., Zhao, L. J., Nesbitt, S. J., Wu, X. C. & Li, C. 2017. A short-snouted, Middle Triassic phytosaur and its implications for the morphological evolution and biogeography of Phytosauria. *Scientific Reports* **7**, 46028.

Stocker, M. R. & Butler, R. J. 2013. Phytosauria. *In* Nesbitt S. J., Desojo J. B. & Irmis R. B. (eds) *Anatomy, phylogeny and palaeobiology of early archosaurs and their kin*, **379**, 91–117. Geological Society, London, Special Publications.

Sues, H.-D., Olsen, P. E., Carter, J. G. & Scott, D. M. 2003. A new crocodylomorph archosaur from the Upper Triassic of North Carolina. *Journal of Vertebrate Paleontology* **23**, 329–43.

Tolchard, F., Nesbitt, S. J., Desojo, J. B., Viglietti, P., Butler, R. J. & Choiniere, J. N. 2019. 'Rauisuchian' material from the lower Elliot Formation of South Africa and Lesotho: Implications for Late Triassic biogeography and biostratigraphy. *Journal of African Earth Sciences* **160**, 103610.

Trotteyn, M. J., Arcucci, A. B. & Raugust, T. 2013. Proterochampsia: an endemic archosauriform clade from South America. *In* Nesbitt S. J., Desojo J. B. & Irmis R. B. (eds) *Anatomy, phylogeny and palaeobiology of early archosaurs and their kin*, **379**, 59–90. Geological Society, London, Special Publications.

Von Baczko, M. B. 2018. Rediscovered cranial material of *Venaticosuchus rusconii* Enables the first jaw biomechanics in Ornithosuchidae (Archosauria: Pseudosuchia). *Ameghiniana* **55**, 365–80.

Von Baczko, M. B. & Desojo, J. B. 2016. Cranial anatomy and palaeoneurology of the archosaur *Riojasuchus tenuisceps* from the Los Colorados Formation, La Rioja, Argentina. *PLoS ONE* **11**, e0148575.

Von Baczko, M. B. & Ezcurra, M. D. 2013. Ornithosuchidae: a group of Triassic archosaurs with a unique ankle joint. *In* Nesbitt S. J., Desojo J. B. & Irmis R. B. (eds) *Anatomy, phylogeny and palaeobiology of early archosaurs and their kin*, **379**, 187–202. Geological Society of London, Special Publication.

Von Baczko, M. B., Desojo, J. B. & Pol, D. 2014. Anatomy and phylogenetic position of Venaticosuchus rusconii Bonaparte, 1970 (Archosauria, Pseudosuchia), from the Ischigualasto Formation (Late Triassic), La Rioja, Argentina. *Journal of Vertebrate Paleontology* **34**, 1342–1356.

Von Baczko, M. B. & Ezcurra, M. D. 2016. Taxonomy of the archosaur *Ornithosuchus*: reassessing *Ornithosuchus woodwardi* Newton, 1894 and *Dasygnathoides longidens* (Huxley 1877). *Earth and*

Environmental Science Transactions of the Royal Society of Edinburgh **106**, 199–205.

Walker, A. D. 1964. Triassic reptiles from the Elgin area: *Ornithosuchus* and the origin of carnosaurs. *Philosophical Transactions of the Royal Society of London, Series B: Biological Sciences* **248**, 53–134.

Watson, D. M. S. 1917. A sketch-classification of the pre-Jurassic tetrapod vertebrates. *Proceedings of the Zoological Society of London* **1917**, 167–86.

Weinbaum, J. C. 2011. The skull of *Postosuchus kirkpatricki* (Archosauria: Paracrocodyliformes) from the Upper Triassic of the United States. *PaleoBios* **30**, 18–44.

Witmer, L. M., Ridgely, R. C., Dufeau, D. L. & Semones, M. C. 2008. Using CT to peer into the past: 3D visualisation of the brain and ear regions of birds, crocodiles and nonavian dinosaurs. *In* Endo, H. & Frey, R. (eds) *Anatomical imaging: towards a new morphology*, 67–87. Tokyo: Springer Verlag.

Zaher, M., Coram, R. A. & Benton, M. J. 2019. The Middle Triassic procolophonid *Kapes bentoni*: computed tomography of the skull and skeleton. *Papers in Palaeontology* **5**, 111–38.

Zittel, K. A. 1887–1890. *Handbuch der Palaeontologie*. 1. Abteilung: Palaeozoologie, 3. Munich and Leipzig. 900 pp.

MS received 15 May 2020. Accepted for publication 24 August 2020. First published online 6 November 2020